C–H and H–H Activation in Transition Metal Complexes and on Surfaces

Jean-Yves Saillard and Roald Hoffmann*

*Contribution from the Department of Chemistry, Cornell University, Ithaca, New York 14853.
Received August 15, 1983*

Abstract: The breaking of the H–H bond in H_2 and a C–H bond in CH_4 on both discrete transition metal complexes and Ni and Ti surfaces is studied, and the essential continuity and similarity of the physical and chemical processes in the two cases is demonstrated. We begin with an orbital analysis of oxidative addition, delineating four basic interactions: H–H or C–H $\sigma \rightarrow M$ electron transfer, the reverse $M \rightarrow \sigma^*$ transfer (both weakening the σ bond, forming the M–H bond), a repulsive interaction between σ and metal filled orbitals, and a rearrangement of electron density at the metal. The molecular cases analyzed in detail are d^6 ML_5, d^8 ML_4 and $CpM'L$. Coordinative unsaturation is necessary, and consequently $\sigma \rightarrow M$ electron transfer dominates the early stages of the reaction. Steric effects are important for the CH_4 reaction. Activation in angular ML_4 or $CpM'L$ is achieved through a destabilized yz MO, and d^{10} ML_3 and ML_2 candidates for activation are described. For our study of the surface we develop tools such as projections of the density of states and crystal orbital overlap populations—the extended structure analogues of a population analysis. These allow a clear understanding of what happens when an H_2 or a CH_4 molecule approaches a surface. Because of the higher energy of the occupied metal orbitals on the surface, the $M \rightarrow \sigma^*$ interaction leads the reaction. There are great similarities and some differences between the activation acts in a discrete complex and on a surface.

In this paper we will try to understand how an H–H or C–H bond can interact and eventually break in the proximity of one or more transition metal centers. We analyze this problem both for discrete complexes and for a clean metal surface; indeed, the most interesting aspect of our study will be the comparison of similarities and differences between the chemistry that goes on in an inorganic complex and on a metal surface.

Let us review the experimental background of this problem. Until recently there was a nice sharp dichotomy in the chemistry of H_2 with transition metal complexes. If H_2 interacted at all, it reacted completely, yielding in an oxidative addition process a metal dihydride, **1**. This species was sometimes observed but


1
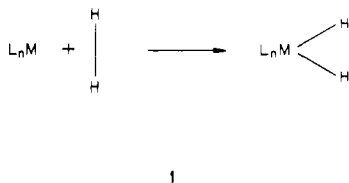
more often inferred as it was consumed rapidly in some subsequent rapid chemistry.[1] Recently the first well-characterized H_2 complex was observed.[2] This is **2**, a side-on bonded complex with

2
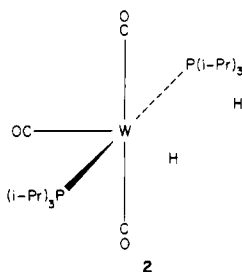
a d^6 ML_5 fragment. The H–H distance, available from a neutron

diffraction study, is 0.75 ± 0.16 Å.

For the interaction of a C–H bond with one or more metal atoms the experimental history is much richer. Over the years it has become apparent that a C–H σ bond can interact in a bonding way with a coordinatively unsaturated metal center (16 or less electrons around the metal) and in so doing allow the metal to achieve or approach the stable 18-electron configuration.[3] Unsaturation at the metal and proximity are required. The intermolecular cases, most of which are quite recent, proceed on to oxidative addition, **3**.[4]

3
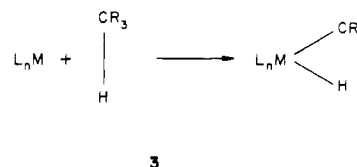
The intramolecular examples, ones in which the interacting alkyl group is somehow tethered to the metal atom, have been revealing in showing us details of the initial stages of metal–CH interaction. There is by now an ample store of structural or spectroscopic evidence for intramolecular M–CH interaction with a variety of geometries, coordination numbers, and electron counts at one or more metal atoms. Precise structure determinations, utilizing

(1) See, for example: James, B. R. "Homogeneous Hydrogenation"; John Wiley & Son, Inc.: New York, 1973, and references therein.

(2) Kubas, G. J.; Ryan, R. R.; Swanson, B. I.; Vergamini, P. J.; Wasserman, H. J. *J. Am. Chem. Soc.* **1984**, *106*, 451–452. Kubas, G. J.; Ryan, R. R.; Vergamini, P. J.; Wasserman, H. "Abstracts of Papers", 185th ACS National Meeting of the American Chemical Society, Seattle, March 1983; American Chemical Society: Washington, DC; INOR 0229; *Chem. Eng. News* **1983**, *20*, March 28, p 4. Another possible case of this type with a d^8 ML_3 fragment is $RhCl(H)_2$ $(P(t-Bu)_3)_2$. Yoshida, T.; Otsuka, S.; Matsumoto, M.; Nakatsu, K. *Inorg. Chim. Acta* **1978**, *29*, 157–159.

(3) (a) Parshall, G. W. *Chem. Soc. Spec. Period. Rpt.* **1977**, *1*, 335–369. Webster, D. E. *Adv. Organomet. Chem.* **1977**, *15*, 147–189. (b) Muetterties, E. L. *Chem. Soc. Rev.* **1982**, *11*, 283–320.

(4) (a) Janowicz, A. H.; Bergman, R. G. *J. Am. Chem. Soc.* **1982**, *104*, 352–354. (b) Jones, W. D.; Feher, F. J. *Ibid.* **1982**, *104*, 4240–4242. (c) Hoyano, J. K.; Graham, W. A. G. *Ibid.* **1982**, *104*, 3723–3725. (d) Shilov, A. E.; Shteinman, A. A. *Coord. Chem. Rev.* **1977**, *24*, 97–144; *Kinet. Katal.* **1977**, *18*, 1129–1145. (e) Baudry, D.; Ephritikhine, M.; Felkin, H. *J. Chem. Soc., Chem. Commun.* **1980**, 1243–1244; **1982**, 606–607. (f) Crabtree, R. H.; Mihelcic, J. M.; Quirk, J. M. *J. Am. Chem. Soc.* **1979**, *101*, 7738–3340. Crabtree, R. H.; Mellea, M. F.; Mihelcic, J. M.; Quirk, J. M. *J. Am. Chem. Soc.* **1982**, *104*, 107–113. (g) Tulip, T. H.; Thorn, D. L. *J. Am. Chem. Soc.* **1981**, *103*, 2448–2450. (h) C–H activation has been shown also with organolanthanides and organoactinide compounds: Watson, P. L. *J. Chem. Soc., Chem. Commun.* **1983**, 176–177. Watson, P. L. *J. Am. Chem. Soc.*, in press. Bruno, J. W.; Marks, T. J.; Day, V. W. *J. Am. Chem. Soc.* **1982**, *104*, 7357–7360. Simpson, S. J.; Turner, H. W.; Andersen, R. A. *Ibid.* **1979**, *101*, 7728–7729. Nizova, G. V.; Krevor, J. V. Z.; Kitaigorodskii, A. N.; Shul'pin, G. D. *Izv. Akad. Nauk. USSR* **1982**, *12*, 2805–2808. (i) Billups, W. E.; Konarski, M. M.; Hauge, R. H.; Margrave, J. L. *J. Am. Chem. Soc.* **1980**, *102*, 7394–7396. Ozin, G. A.; McIntosh, D. F.; Mitchell, S. A. *Ibid.* **1981**, *103*, 1574–1575. Ozin, G. A.; McCaffrey, J. G. *Ibid.* **1982**, *104*, 7351–7352. Klabunde, J. J.; Tanaka, Y. *Ibid.* **1983**, *105*, 3544–3546.

neutron diffraction, show short M to H (and C) contacts, and unusually long C–H bonds (the world's record now stands at 1.19 Å[5]). C–H stretching frequencies often are dramatically lowered and C–H coupling constants as well. There is evidence of both linear, **4a**, and triangular, **4b**, interaction geometries.

4
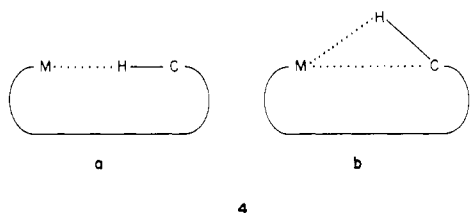
H₂ and alkanes are, of course, chemisorbed, dissociated, and reassembled on many transition metal surfaces of varying degrees of cleanliness. In recent times the reactivity of definite crystal planes has been studied in some detail, and we are beginning to gain information on the microscopic structure of the product surface.[6]

Theoretical studies of surfaces and their interaction with molecules are now being done by several groups. We want to single out for special mention here the work of Baetzold, Shustorovich, and Muetterties[7] because it anticipates many of the

(5) (a) For a review on CH–transition metal bonds, see: Brookhart, M.; Green, M. L. H. *J. Organomet. Chem.* **1983**, *250*, 395–408. (b) Otsuka, S.; Yoshida, T.; Matsumoto, M.; Nakatsu, K. *J. Am. Chem. Soc.* **1976**, *98*, 5850–5858. (c) Yared, Y. W.; Miles, S. L.; Bau, R.; Reed, C. A. *Ibid.* **1977**, *99*, 7076–7078. (d) Roe, D. M.; Bailey, P. M.; Moseley, K.; Maitlis, P. M. *J. Chem. Soc., Chem. Commun.* **1973**, 1273–1274. (e) Mann, B. E.; Bailey, P. M.; Maitlis, P. M. *J. Am. Chem. Soc.* **1975**, *97*, 1275–1276. (f) Echols, H. M.; Dennis, D. *Acta Crystallogr., Sect. B* **1976**, *B30*, 2173–2176. (g) Echols, H. M.; Dennis, D. *Ibid.* **1975**, *B32*, 1627–1630. (h) Van Der Poel, H.; van Koten, G.; Vrieze, K. *Inorg. Chem.* **1980**, *19*, 1145–1151. (i) Postel, M.; Pfeffer, M.; Riess, J. G. *J. Am. Chem. Soc.* **1977**, 5623–5627. (j) Dehand, J.; Fisher, J.; Pfeffer, M.; Mitschler, A.; Zinzius, M. *Inorg. Chem.* **1976**, *15*, 2675–2681. (k) Van Baar, J. F.; Vrieze, K.; Stufkens, D. J. *J. Organomet. Chem.* **1974**, *81*, 247–259. (l) Bailey, N. A.; Jenkins, J. M.; Mason, R.; Shaw, B. L. *J. Chem. Soc., Chem. Commun.* **1965**, 237–238. (m) La Placa, S. J.; Ibers, J. A. *Inorg. Chem.* **1965**, *4*, 778–783. (n) Cotton, F. A.; La Cour, T.; Stanilowski, A. G. *J. Am. Chem. Soc.* **1974**, *96*, 754–759. (o) Cotton, F. A.; Day, V. W. *J. Chem. Soc., Chem. Commun.* **1974**, 415–416. (p) Cotton, F. A.; Stanislowski, A. G. *J. Am. Chem. Soc.* **1974**, *96*, 5074–5082. (q) Harlow, R. L.; McKinney, R. J.; Ittel, S. D. *Ibid.* **1979**, *101*, 7496–7504. (r) Brown, R. K.; Williams, J. M.; Schultz, A. J.; Stucky, G. D.; Ittel, S. D.; Harlow, R. L. *Ibid.* **1980**, *102*, 981–986. (s) Brookhart, M.; Lamanna, W.; Humphrey, M. B. *J. Am. Chem. Soc.* **1982**, *104*, 2117–2126. (t) Schultz, A. J.; Teller, R. G.; Beno, M. A.; Williams, J. M.; Brookhart, M.; Lamanna, W.; Humphrey, M. B. *Science* **1983**, *220*, 197–199. (u) Dawoodi, Z.; Green, M. L. H.; Mtetwa, V. S. B.; Prout, K. *J. Chem. Soc., Chem. Commun.* **1982**, 802–803, 1410–1411. (v) Schultz, A.; Williams, J. M.; Schrock, R. R.; Rupprecht, G.; Fellmann, J. D. *J. Am. Chem. Soc.* **1979**, *101*, 1593–1594. (w) Calvert, R. B.; Shapley, J. R. *Ibid.* **1978**, *100*, 7726–7727. (x) Dawkins, G. M.; Green, M.; Orpen, A. G.; Stone, F. G. A. *J. Chem. Soc., Chem. Commun.* **1982**, 41–43. (y) Beno, M. A.; Williams, J. M.; Tachikawa, M.; Muetterties, E. L. *J. Am. Chem. Soc.* **1981**, *103*, 1485–1492.

(6) (a) For a general review of surface chemistry, see: Somorjai, G. A. "Chemistry in Two Dimensions: Surfaces"; Cornell University Press: Ithaca, 1981. For a review of H₂ on transition metal surfaces, see: Burch, R. *Chem. Phys. Solids: Their Surfaces* **1980**, *8*, 1–7. (b) Maire, G.; Anderson, J. R.; Johnson, B. B. *Proc. R. Soc. London, Ser. A* **1970**, *320*, 227–250. (c) Schouten, F. C.; Kaleveld, E. W.; Bootsma, G. A. *Surf. Sci.* **1977**, *63*, 460–474. (d) Firment, L. E.; Somorjai, G. A. *J. Chem. Phys.* **1977**, *66*, 2901–2913. (e) Salmeron, M.; Somorjai, G. A. *Ibid.* **1981**, *85*, 3635–3840. (f) Madey, T. E.; Yates, J. R. *Surf. Sci.* **1978**, *76*, 397–414. (g) Wittrig, T. S.; Szuromi, P. D.; Weinberg, W. H. *J. Chem. Phys.* **1982**, *1*, 116–123, 3305–3315. (h) Tsai, M. C.; Friend, C. M.; Muetterties, E. L. *J. Am. Chem. Soc.* **1982**, *104*, 2539–2543. (i) Karpinsky, Z. *J. Catal.* **1982**, *77*, 118–137. (j) Yates, J. T., Jr.; Zinck, J. J.; Sheard, S.; Weinberg, W. H. *J. Chem. Phys.* **1979**, *70*, 2266–2272. (k) Hoffmann, F. M.; Felter, T. E.; Weinberg, W. H. *J. Chem. Phys.* **1982**, *76*, 3799–3808. (l) Felter, T. E.; Hoffmann, F. M.; Thiel, P. A.; Weinberg, W. H. *Surf. Sci.*, in press. (m) Hoffmann, F. M.; Felter, T. E.; Thiel, P. A.; Weinberg, W. H. *Ibid.*, in press. (n) Weinberg, W. H. *Surv. Prog. Chem.* **1983**, *10*, 1–59. (o) Somorjai, G. A. In "Robert A. Welch Foundation Conference on Chemical Research. XXV. Heterogeneous Catalysis", 1981; pp 83–138. (p) Demuth, J. E.; Ibach, H.; Lehwald, S. *Phys. Rev. Lett.* **1978**, *40*, 1044–1047.

(7) (a) Baetzold, R. *J. Am. Chem. Soc.* **1983**, *105*, 4271–4276. Shustorovich, E. *J. Phys. Chem.* **1983**, *87*, 14–17. Shustorovich, E.; Baetzold, R.; Muetterties, E. L. *J. Phys. Chem.* **1983**, *87*, 1100–1113. (b) Shustorovich, E. *J. Am. Chem. Soc.* **1980**, *102*, 5989–5993; *J. Phys. Chem.* **1982**, *86*, 3114–3120; *Solid State Commun.* **1982**, *44*, 567–572. See also ref 3b.

conclusions that we eventually reach about the surface, in particular concerning the role of the substrate σ* orbitals and the direction of electron flow during surface–substrate interaction. Other theoretical studies will be mentioned in the course of the paper.

Charge Transfer and Bond Making in Oxidative Addition

At the risk of repeating what is obvious let us examine the essential features of oxidative addition, correlating the basic ideas of electron transfer and oxidation, reduction with the way in which these appear in a molecular orbital description of this process.[8]

Drawing **5** is a schematic illustration of the level transformation in a transition metal complex reacting with H₂. The MLₙ complex

5
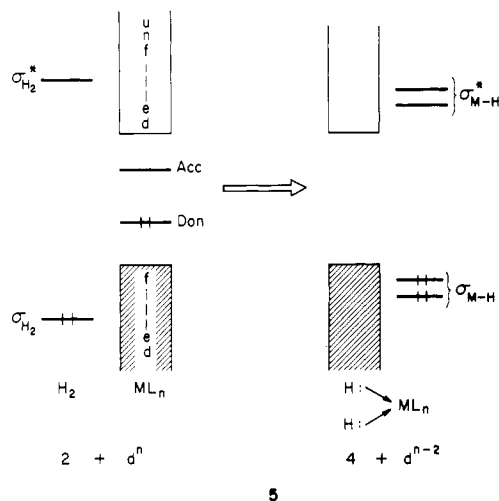
is represented by a band of occupied levels and a band of unoccupied ones. The metal surface will be no different. One of the metal-filled levels (Don for Donor) and one of the unfilled ones (Acc for Acceptor) is singled out, for reasons which will soon become apparent. At the end of the reaction two new M–H σ bonds form, and of course their corresponding antibonding combinations. In the conventional Wernerian scheme of counting ligands as two-electron σ donors, the four electrons of the two new M–H σ bonds are assigned, for electron-counting purposes, to the ligands, H⁻. It is this convention which makes the metal go from a dⁿ to a dⁿ⁻² electron count and makes us call this reaction an oxidative (at the metal) addition.

Formalisms are convenient fictions which contain a piece of the truth—and it is so sad that people spend a lot of time arguing about the deductions they draw, often ingeniously and artfully, from formalisms, without worrying about their underlying assumptions. The "complex" or dative bonding picture which led to "oxidation at metal" of course is an exaggeration. The M–H σ bonds are in good part covalent. To the extent that they are so, the real d electron population at the metal moves back from dⁿ⁻² toward dⁿ. To the extent that it probably never quite gets back to dⁿ it is still informative to call this an oxidative addition.

What the "oxidative addition" formalism conceals and a molecular orbital picture reveals is that in the course of this reaction there has to be a two-way flow of electron density, from the metal to the new ligands and in the reverse direction.

Consider the M–H σ bonds in the product. In a localized representation they are shown in **6**, and the equivalent delocalized picture in **7**. The delocalized orbitals are labeled as S or A according to their symmetry or antisymmetry with respect to the twofold axis or mirror that interchanges them.

Where did **7S** and **7A** originate? They came from the interaction of σ_H₂ with metal Acc and metal Don with σ*_H₂. This is shown in **8** and in another way, focussing on the evolution of the orbitals, in **9**. What **9** shows clearly is the two-way charge transfer

(8) For an illuminating discussion of this problem, see: Crabtree, R. H.; Hlatky, G. G. *Inorg. Chem.* **1980**, *19*, 571–572.

6   **7**

8

9

10
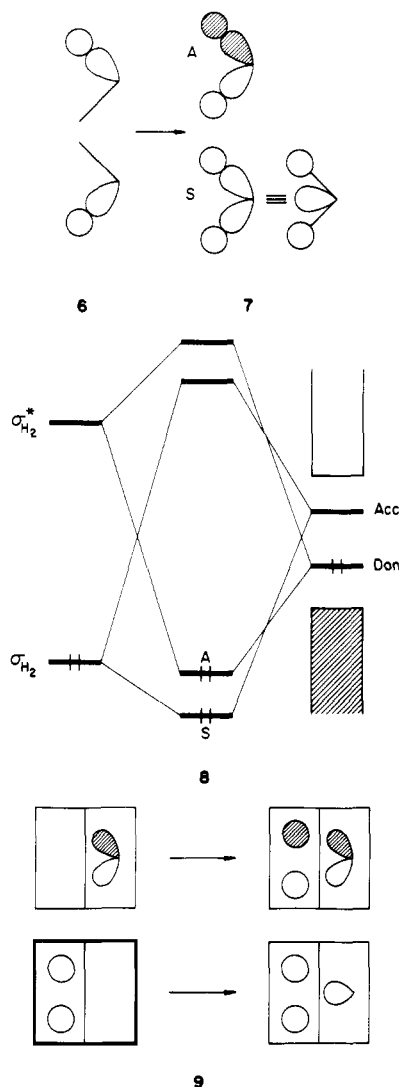
and the coupling of electron transfer and bonding changes. The symmetric M–H combination evolves from σ_{H_2} by mixing in of a metal acceptor orbital of appropriate symmetry. The result is electron transfer *from* H_2 σ, decreased H–H bonding, and increased M–H bonding. The A combination electron transfer is in the opposite direction, for this orbital is originally on the metal. Electron transfer *to* H_2 σ^* has as a consequence decreased H–H bonding and increased M–H bonding.

Note that both of these interactions lead to H–H bond weakening and M–H bond formation, even though they accomplish these actions by charge transfer in different directions.

The molecular orbital description makes it clear that when oxidative addition is complete there must have occurred electron transfer from metal to H_2 or RH *and* in the reverse direction. But there is no requirement that the electron flow be balanced at every stage of the reaction. In fact, the experimental evidence for the requirement of coordinative unsaturation of the metal in activation on discrete complexes makes it clear that in these molecules the important initial electron flow is from H_2 to metal. As we will see, metal surfaces may be different.

So far we have identified the two most important bonding interactions between a hydrogen molecule or an alkane and a discrete transition metal complex or a metal surface. They are repeated in **10**, labeled as ① and ② now. These are two-orbital two-electron bonding interactions. Two further interactions must be thought about. Interaction ③ is the two-orbital four-electron perforce destabilizing interaction between filled orbitals of substrate and surface (or complex). It is in this interaction that one-electron theories of the extended Hückel type find what chemists normally call "steric effects". Interaction ③ is destabilizing, and it leads to some M–H antibonding. It is the primary
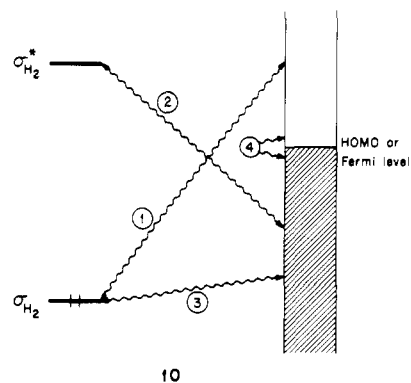
source of barriers to C–H activation.

In addition to these three interactions, which operate for an ML_n complex as well as for a metal surface, there is another interaction, ④, which is generally important only for metal surfaces, where there are many closely spaced levels. What happens on the surface, as we will see in great detail below, is that some levels, more localized on the surface than in the bulk, and even on the surface distinguished by reaching out toward the substrate, interact to a greater extent than others. They do so, of course, through the primary interactions ①, ②, and ③. But since in a solid or a surface levels are closely spaced around the Fermi level, the net result of such primary interactions of substrate and "surface states" is a shift of electron density between bulk and surface, and even within the surface. This interaction is poorly represented in **10** by ④, but its significance will eventually become clearer as we describe it in more detail later.

We are now ready to proceed with an analysis of several specific cases, to see these interactions in action. But first let us describe the computational methodology we use. This is the extended Hückel method,[9] with particulars described in Appendix I. There is a special problem which this transparent and simple procedure brings with it. The method is not reliable for bond distance changes, and H_2 in particular is a pathological case in which the two atoms collapse. So the study of potential energy surfaces where H–H or C–H bonds are made or broken would seem to be an inappropriate application of the extended Hückel method. In fact this is so, and since we cannot trust the method for bond distances, we do not calculate complete potential energy surfaces. Instead we limit ourselves in general to the study of select approaches—for instance an H_2 coming on parallel or perpendicular to a surface—and focus on that aspect of the electronic redistribution which the extended Hückel method from our experience is likely to get right. This is the magnitude and nodal character of orbital interactions.

We also apply consistently the language and formalism of simple perturbation theory, in particular the second-order expression for the interaction of two levels:

$$\Delta E = \frac{|H_{ij}|^2}{E_i^0 - E_j^0}$$

Extended Hückel arguments, especially in the fragment orbital analysis, translate directly into perturbation arguments. It is this combination of extended Hückel calculations and perturbation theory based thinking within a one-electron frontier orbital picture that makes us feel more sanguine about the results of what would otherwise have been a pretty unreliable calculation.

H_2 and CH_4 as Substrates

The orbitals of both molecules are familiar. Within a simple single configuration picture the valence orbitals are filled σ_g in H_2, an $a_1 + t_2$ set in CH_4, and the corresponding unfilled σ_u^* in H_2 and a_1^* and t_2^* in CH_4. The orbital energies as given by the

(9) (a) Hoffmann, R. *J. Chem. Phys.* **1963**, *39*, 1397–1412.   (b) Hoffmann, R.; Lipscomb, W. N. *Ibid.* **1962**, *36*, 2176–2195.
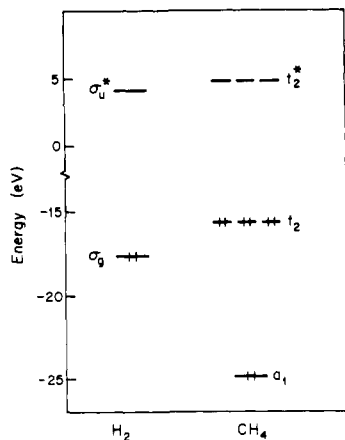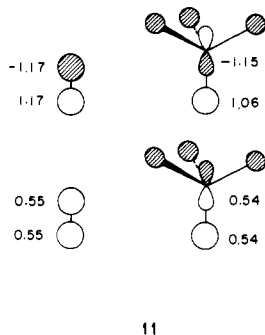
C-H and H-H Activation in Transition Metal Complexes

J. Am. Chem. Soc., Vol. 106, No. 7, 1984 2009

Figure 1. Frontier orbitals of H_2 and CH_4.

Figure 2. Total energy along the perpendicular and parallel approaches of H_2 to $Cr(CO)_5$. The common energy zero for both curves is for the two fragments at infinite separation.

extended Hückel method are shown in Figure 1. The C–H bonding in CH_4 is distributed over the a_1 and t_2 set, but it is mainly in the t_2 component. If we focus on that orbital as the C–H bond and then compare CH_4 and H_2 then, as far as energetics are concerned, the two molecules are equally good (poor) acceptors, but CH_4 is a better (but still not good) donor, as its t_2 set is some 2 eV higher in energy than H_2 σ.

The numerator of the perturbation sum, $|H_{ij}|^2$, is not to be forgotten. Coefficients of the relevant orbitals are given in **11**. Note first the spectacular difference between the σ_g and σ_u^* H coefficients in H_2. This is a result of including the overlap in

11

the normalization of the molecular orbitals. An immediate consequence is that σ^* orbitals, acting through the numerator of the perturbation expression, will have much more "power" in the interaction. This will compensate sometimes (as we will see, especially on transition metal surfaces) for their very high energy, which, acting through the denominator of the perturbation expression, makes it difficult for them to have much influence. Note the similarity of the effective H coefficients in CH_4 and H_2.

We are now ready to proceed with calculations on the addition of these molecules to various ML_n fragments. The reader should note that our calculations are not the only ones extant and that several others have been published.[10]

Figure 3. Interaction diagram for H_2 and $Cr(CO)_5$ for a perpendicular (left) and parallel (right) approach. The diagram is schematic in the position of the σ_g and σ_u^* levels before and after interaction.

A Prototype Mononuclear Transition Metal Fragment, $Cr(CO)_5$

Why $Cr(CO)_5$? Complexes of $Cr(CO)_5$ with methane and hexane in low-temperature matrices have been detected.[11] The only well-characterized H_2 complexes $M(CO)_3(PR_3)_2H_2$, M = Mo, W, are closely related to $Cr(CO)_5^2$, and many of the cited intramolecular cases of C–H activation can be related back to this model.[5l–t]

The total energy of an H_2 frozen at H–H = 0.74 Å approaching a C_{4v} octahedral fragment $Cr(CO)_5$ is shown in Figure 2. Two approach geometries were studied, a "perpendicular" and a "parallel" mode. These are sufficiently common in the subsequent discussion that it is best to describe them more precisely in **12** and **13**. "Perpendicular" means H–H (or eventually C–H) colinear with the metal atom and "parallel" means turned by 90°, so that both M–H distances are equal. The L_nM–H_2 separation,

(10) (a) Sevin, A. Nouv. J. Chim. **1981**, 5, 233–241. Sevin, A.; Chaquin, P. Ibid. **1983**, 7, 353–360. (b) Dedieu, A.; Strich, A. Inorg. Chem. **1979**, 18, 2940–2943. (c) Kitaura, K.; Obara, S.; Morokuma, K. J. Am. Chem. Soc. **1981**, 103, 2892–2893. Obara, S.; Kitaura, K.; Morokuma, K., to be published. (d) Shestakov, A. F. Koord. Khim. **1980**, 6, 117–123. (e) Gritsenko, O. V.; Bagaturyants, A. A.; Moiseev, I. I.; Kazanskii, V. B.; Kalechits, I. V. Kinet. Katal. **1980**, 21, 632–638. Kuzminskii, M. B.; Bagaturyants, A. A.; Zhidomirov, G. M.; Kazanskii, V. B. Ibid. **1981**, 22, 354–358. Gritsenko, O. V.; Bagaturyants, A. A.; Moiseev, I. I.; Kalechits, I. V. Ibid. **1981**, 22, 1431–1437. Bagaturyants, A. A.; Anikin, N. A.; Zhidomirov, G. M.; Kazanskii, V. B. Zh. Fiz. Khim. **1981**, 55, 2035–2039; **1982**, 56, 3017–3022. Anikin, N. A.; Bagaturyants, A. A.; Zhidomirov, G. M.; Kazanskii, V. B. Ibid. **1982**, 56, 3003–3007. Lebedev, V. L.; Bagaturyants, A. A.; Zhidomirov, G. M.; Kazanskii, V. B. Ibid. **1983**, 57, 1057–1067. Bagaturyants, A. A. Ibid. **1983**, 57, 1100–1106. (f) Noell, J. O.; Hay, P. J. J. Am. Chem. Soc. **1982**, 104, 4578–4584. Hay, P. J. Chem. Phys. Lett. **1984**, 103, 466–469. (g) Blomberg, M. R. A.; Siegbahn, P. E. M. J. Chem. Phys. **1983**, 78, 986. Brandemark, U. B.; Blomberg, M. R. A.; Petterson, L. G. M.; Siegbahn, P. E. M. J. Phys. Chem., in press.
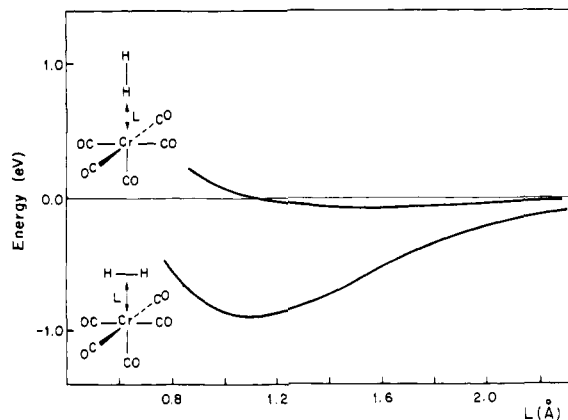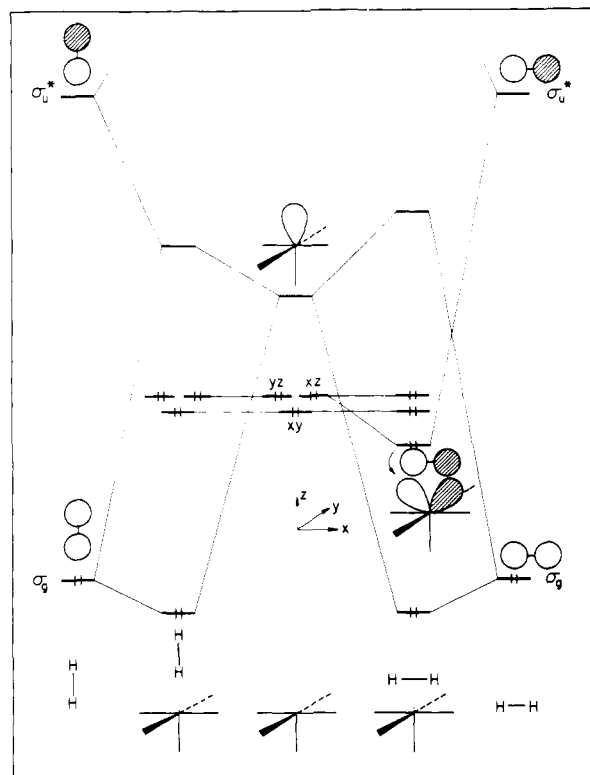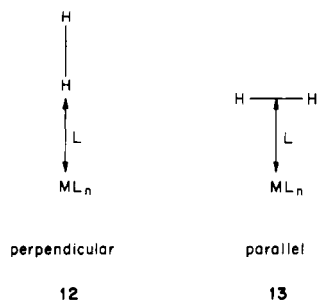
(11) Graham, M. A.; Perutz, R. N.; Poliakoff, M.; Turner, J. J. J. Organomet. Chem. **1982**, 34, C34 (1972). Welch, J. A.; Peters, K. A.; Vaida, V. J. Phys. Chem. **1982**, 86, 1941–1947.

12   **13**

perpendicular   parallel

Figure 4. Total energy for perpendicular and parallel approaches of CH_4 to $Cr(CO)_5$. The common energy zero for both curves is for both fragments at infinite separation.

somewhat arbitrarily, is defined as the distance to near hydrogen in the perpendicular geometry, but to the H–H centroid in the parallel form.

The two energy curves are attractive over a substantial range of approach distances, and the parallel minimum is deeper. This is consistent with the single structure known, **2**, but why is it so?

A level interaction diagram (Figure 3) is illuminating. Singled out in the middle of the construction are the familiar orbitals of a 16-electron C_{4v} ML_5 fragment—a t_{2g} set below a well-directed a_1 hybrid.[12]   In the perpendicular geometry the t_{2g} set is untouched, while both σ_g and $\sigma_u{}^*$ interact in a typical three-orbital pattern with ML_5 a_1. The significant bonding mixing is of type ① in **10**, between σ_g and a_1 of $Cr(CO)_5$ in Figure 3. It gives rise to stabilization, but the stabilization is not great as it is underlain by a repulsive base of four-electron destabilizing interactions.

In the parallel geometry the interaction between σ_g and a_1, though somewhat different in spatial configuration, in fact is not significantly worse in overlap. Now a strong interaction of type ②, metal acting as a donor (xz) toward the ligand as acceptor $(\sigma_u{}^*)$, is allowed by symmetry, whereas it was forbidden in the perpendicular approach. There is electron transfer from σ (0.110 electrons at $L = 2.0$ Å) and into σ^* (0.032 electrons at $L = 2.0$ Å). No wonder the parallel geometry is preferred.

The situation is changed dramatically if the H–H bond is substituted by C–H of CH_4 (Figures 4 and 5). The perpendicular approach is still attractive, but the parallel one is not, becoming strongly repulsive. The level analysis reveals that the origin of stabilization in the perpendicular approach is the same for CH_4 as H_2. In the parallel geometry something different is happening, for instead of xz going down in energy (H_2), in the case of methane both xz and yz go up. The reason for this behavior may be seen from the fragment overlaps (at $L = 2.0$ Å) in **14**. The H_2 xz–σ^*


$\langle xz \mid \sigma_u{}^* \rangle = 0.15$ $\langle xz \mid \sigma^* \rangle = 0.04$

14 $\langle xz \mid \sigma \rangle = 0.08$
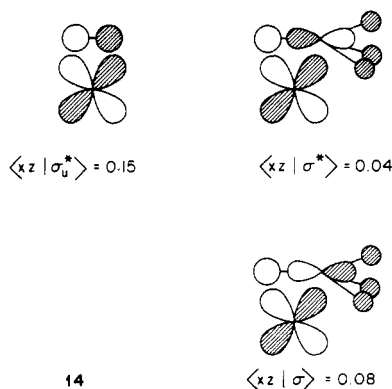
overlap is big, but that of the corresponding σ^* component of CH_4 is small. The metal d orbital is mismatched with the methane, and samples the rear of the CH σ^* combination. Furthermore, there is a substantial overlap between metal xz and the *occupied* C–H σ orbital. In fact, this repulsive effect dominates, pushing xz up in energy (Figure 5) as it interacts more with C–H σ than with σ^*. The metal yz orbital also goes up as a result of a similar four-electron destabilization with another member of the t_2 set.

What we have is the dominance of two-orbital four-electron repulsions over the attractive bonding forces. We think that we
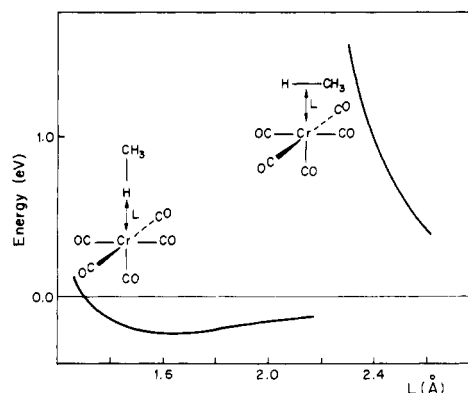
(12) Elian, M.; Hoffmann, R. *J. Am. Chem. Soc.* **1975**, *14*, 1058–1076.
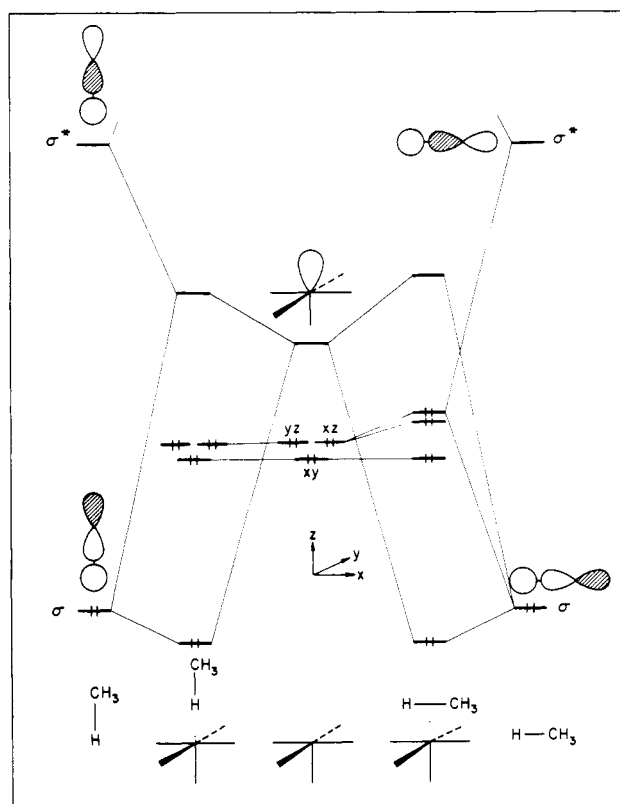
Figure 5. Interaction diagram, schematic at the top and bottom of the energy range, for perpendicular (left) and parallel (right) approaches of CH_4 to $Cr(CO)_5$.
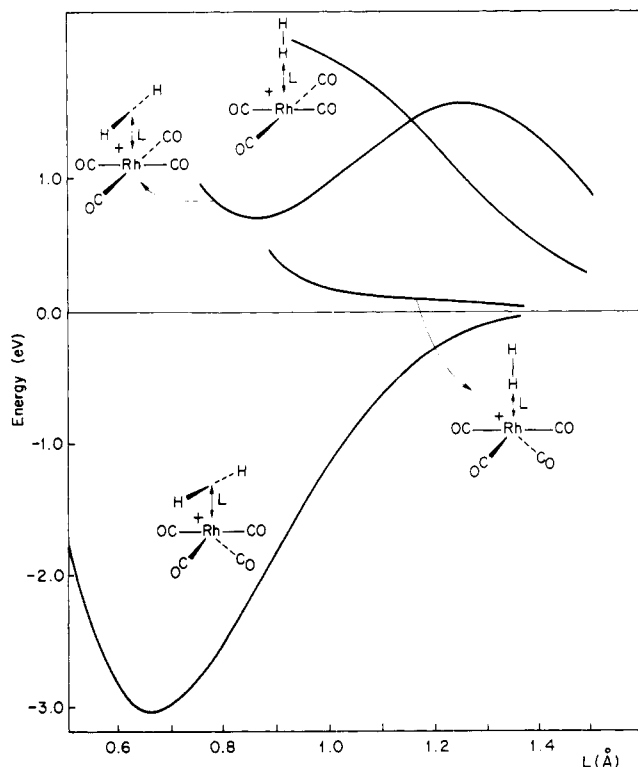
can identify the repulsive effects, as safely as one can do it within the framework of a one-electron theory, with steric effects.

Thus, when a methane approaches a $Cr(CO)_5$ in a parallel geometry the steric problems of that approach overrule the favorable geometric arrangement. Rotation of the methyl group around the H–C bond does not alleviate the trouble. Can a geometry intermediate between parallel and perpendicular achieve a compromise?

We tried **15** and **16**, in various geometries. Stabilization was

15   16
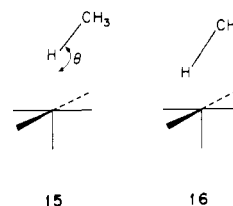
achieved for some geometries, for instance at M–H = 2.0 Å, **15** is bound for all $\theta \leq 130°$. But the perpendicular configuration,

C-H and H-H Activation in Transition Metal Complexes

J. Am. Chem. Soc., Vol. 106, No. 7, 1984 2011

Figure 6. Total energy for perpendicular and parallel approaches of H_2 to a square-planar and angular $Rh(CO)_4{}^+$. The common energy zero for all curves is at infinite separation of the fragments.

$\theta = 180°$, is most stable. These are intermolecular cases, and we are certain that in special intramolecular geometries, where the C-H bond is so suspended near the metal that steric effects are minimized, that an appropriate triangular geometry with partial M-H and M-C bonding is attainable.

A particularly interesting example of intramolecular interaction occurs in the series of 16-electron, near-octahedral complexes of type **17**. These exhibit short M···H and M···C contacts associated
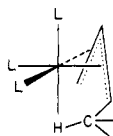
17

with fluxional behavior of the H atom.[5a,t-v] Previous extended Hückel calculations on the model $[Co(\eta^3\text{-alkenyl})(PH_3)_3]^{2+}$ have pointed out a low-lying orbital in which both M···H and M···C interactions are bonding.[5q] Our calculation on the isoelectronic $[Fe(\eta^3\text{-alkenyl})(CO)_3]^+$ complex shows similar results: two relatively delocalized σ_{CH} orbitals of the methyl group are stabilized by the metal LUMO. In the two corresponding bonding MO's, the overlap populations are 0.060 for M-H and 0.030 for M-C. The corresponding values for the total overlap populations are 0.075 and 0.006, respectively. Despite the short M-C distance, there is weak interaction. The reason is that the bonding attraction between the accepting hybrid orbital and the σ_{CH} bond is balanced by a secondary M-C antibonding effect, a consequence of the bonding interaction between the metal orbital and the polyenyl π system.

d^8 ML_4 and CpML Systems for Activating C-H Bonds

Short M-H contacts have been shown to exist in planar or near planar 16-electron complexes of type **18**.[5d-k] Although the accuracy of the H atom positions is poor, the X-ray crystallographic results suggest that the M-H distances lie in the range 2.3-3.0 Å,[5d-f,j] substantially longer and weaker than the corresponding distances in ML_5 complexes. More interesting, perhaps, is the fact that we can place in the d^8 ML_4 category the recent exciting

18   19
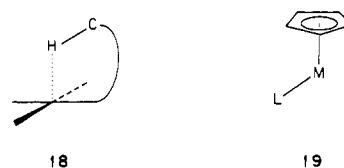
cases of C-H activation using the CpML fragment, M = Rh, Ir, **19**.[4a-c]

Our model study examined the approach of H_2 and CH_4 to square-planar and angular $Rh(CO)_4{}^+$ fragments, **20** and **21**.
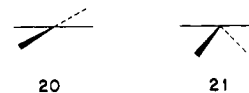

20   21

Figure 6 shows the computed total energy curves for H_2. Both approaches to the square-planar fragment are repulsive. At large separations the perpendicular approach is preferred, in agreement with previous calculations by Sevin[10a] and by Dedieu and Strich.[10b] When the square-planar fragment **20** is bent back to the angular one **21**, the parallel approach is greatly stabilized.

The reasons for this behavior are made clear by examining the frontier orbitals of **20** and **21**,[13] and comparing them to those of the ML_5 fragment, $Cr(CO)_5$. This is done in **22**. The crucial
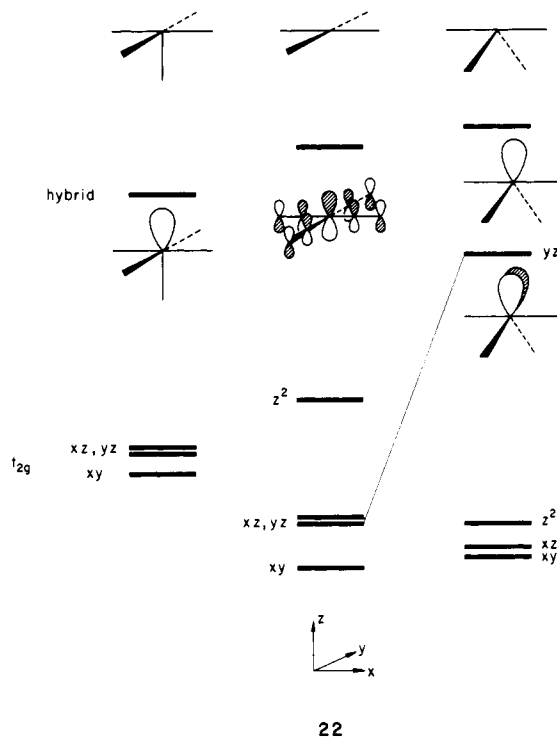
22

difference between d^8 square-planar ML_4 and d^6 ML_5 is the presence of the occupied z^2 in the former and the very different makeup of the LUMO. The z^2 orbital introduces an additional high-lying orbital of axial symmetry, capable of interaction with σ and σ^* of H_2 in the perpendicular geometry and with σ in the parallel one. The dominant effect is the four-electron destabilizing one, and this is what makes the two square-planar approaches in Figure 6 unfavorable. The acceptor orbital of ML_4 is a poor counterpart of the ML_5 hybrid. The ML_4 orbital which is the LUMO is only 15% metal p, and predominantly ligand π^*. Not surprisingly, given what we know about the chemistry of square-planar d^8 complexes, the coordinative unsaturation or acceptor power of square-planar ML_4 is not strongly developed.

Much changes when two trans ligands in square-planar ML_4 are bent back to give the angular fragment **21**. The LUMO becomes a hybrid more localized on the metal, and resembling more the LUMO of ML_5. And most importantly the yz orbital,

---

(13) See ref 12 for the orbitals of ML_4.

the one which lies in both the plane of deformation and the plane of H_2 approach, is destabilized (thus moving it closer in energy to σ_u^* of H_2, with which it interacts) and hybridized away from the fragment (thus providing better overlap with σ_u^* of H_2). It is no wonder the stabilization shown in Figure 6 is so great—one has moved part-way toward the product geometry of oxidative addition. The deformation toward an angular fragment has activated ML_4 for the reaction, a pointed noted and discussed in detail by Sevin and by Dedieu and Strich.[10] We will soon see the relationship of this phenomenon to the observation of CH activation by CpML intermediates.

We have also calculated potential energy curves for the approach of methane to $Rh(CO)_4^+$. The perpendicular approaches resemble those of H_2. The parallel ones are dominated by steric repulsion, so much so that even the very attractive approach of H_2 to angular ML_4 is transformed into a repulsive one in the case of methane.

The observation of short M–H contacts in complexes of type **18** seems in disagreement with our repulsive curves of Figure 6. One could argue that this is the consequence of the choice of carbonyl ligands in our model calculations. Complexes of the type **18** always carry donor ligands such as phosphines or halides. So we did the same calculations, replacing the four carbonyls by chlorides. This substitution in planar ML_4 fragments is well known. The main result is a moderate destabilization of the t_{2g} set (xy, xz, yz) and a large destabilization of z, which, however, becomes 85% localized on the metal. The z^2 orbital remains unchanged. As the interaction between ML_4 and H_2 or CH_4 is dominated by the z^2 σ_{H_2} repulsion, the four $E = f(L)$ curves still remain repulsive, even if they are less so.

A careful examination of the structures of type **18** shows that their M–C chains, because of their steric encumbrance and their partial rigidity, are forced to lie in a plane roughly perpendicular to the ML_4 plane, bringing a C–H bond in proximity to the metal. The compounds will minimize M···C–H repulsion by bringing the H atom into an axial position (leading to a positive M···H overlap population) and the C atom as far away as possible (thus minimizing the M···C negative overlap population). Our calculations on the model **23** give overlap population values of +0.025 for
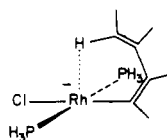

23

Rh–H and –0.094 for Rh–C, the corresponding interatomic distance being respectively 1.78 and 2.75 Å. The total M–(H–C) overlap population is negative, in agreement with a corresponding destabilizing interaction. Our conclusion is in agreement with the structural work of Echols and Dennis,[5g] who suggested that in the planar pyrozolyl Ni complexes, there is no M···H short contact if the molecule is sterically free to avoid it.

Our next goal is to understand the activation of methane by CpML intermediates, such as are thought to be created in the studies of Bergman, Graham, Jones, and their co-workers. From a theoretical point of view the isolobal analogy d^8 ML_4 ⟷ d^8 CpM′L, **24** ⟷ **25** is obvious,[14] but does it in fact hold up?
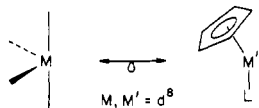

24   **25**

(14) We assume a low-spin-singlet configuration for both ML_4 and CpM′L. For the orbitals of CpML and a discussion of its geometry and spin states, see: Hofmann, P.; Padmanabhan, M. *Organometallics* **1983**, *2*, 1273–1284. See also: Veillard, A.; Dedieu, A. *Theor. Chim. Acta*, in press.
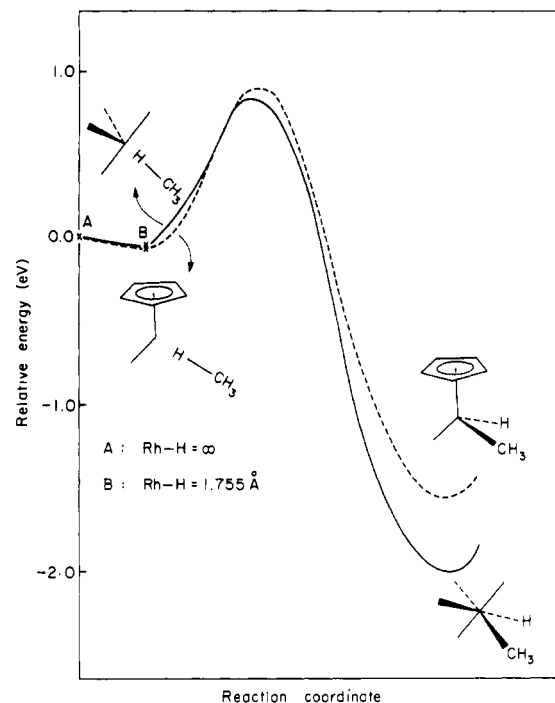
Figure 7. A comparison of computed potential energy curves for hypothetical oxidative addition reaction coordinates of CH_4 to CpRh(CO) and $Rh(CO)_4^+$. Both molecules are referred to the same energy zero when at infinite separation.

To answer this question we constructed a hypothetical reaction coordinate for the oxidative addition of CH_4 to $Rh(CO)_4^+$ and CpRhCO, **26**. We are not able, as we said above, to calculate
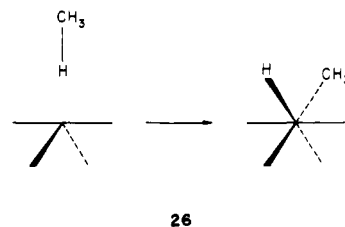
26

a realistic path with the extended Hückel method. Better calculations will have to do that. What we did was make a linear transit between a point on the perpendicular approach (Rh–H = 1.755 Å, corresponding to the minimum on the $E(L)$ curve) and an idealized octahedral product geometry (Rh–H = 1.6 Å, Rh–C = 1.95 Å). The transit is certainly not optimal, but it does contain the essential features of any reasonable reaction coordinate, for instance reorientation of the methyl group to point toward the metal.

A glance at Figure 7, the comparison of the CpRhCO(CH_4) and $Rh(CO)_4^+$(CH_4) transits, shows how well the isolobal analogy works. Great similarity is also seen in the Walsh diagram for the two cases. Given the validity of the analogy we would like to go back to the somewhat more symmetrical $Rh(CO)_4^+$ model to see how activation comes about.

A diagram showing the evolution of the critical energy levels along the reaction coordinate, i.e., a simplified Walsh diagram for angular $Rh(CO)_4^+$ and CH_4, is shown in Figure 8. The interacting fragment levels are not much perturbed in the beginning of the reaction (left side of Figure 8). Compare with **22**: at low energy in ML_4 + CH_4 are xz, xy, and z^2, higher is the occupied yz. The final product is a typical octahedral complex with an occupied t_{2g} set. One of the bunch of four highest occupied orbitals is mostly metal–H, CH_3 bonding.

When we use a square-planar ML_4 fragment, the calculated barrier to oxidative addition is substantially higher. We can trace the difference, i.e., the lowering of the activation energy when addition takes place to the angular fragment (or to CpML), to
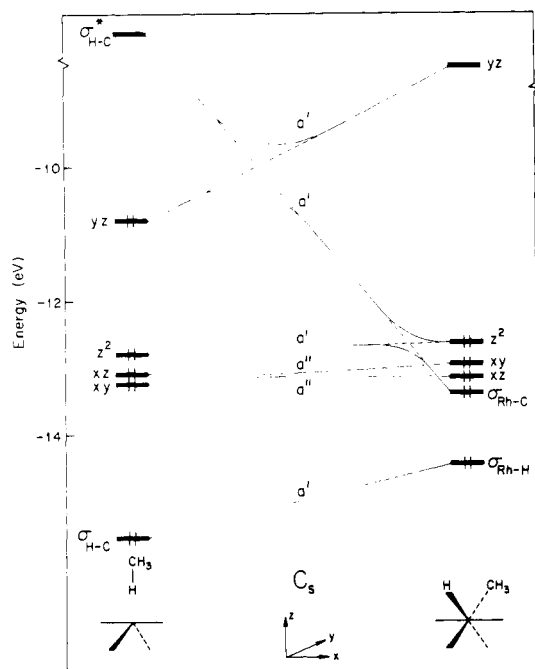
Figure 8. The evolution of the important energy levels along the oxidative addition reaction coordinate for $Rh(CO)_4^+$ and CH_4.

the higher energy of the yz orbital in the latter.

It is worthwhile at this point to draw the necessary connection between oxidative addition and its microscopic reverse, reductive elimination. The latter reaction has been studied theoretically in some detail by us and by others.[15] The essence of what happens in reductive elimination is that one of the two M–R σ bond combinations goes down to the new R–R σ bond, **27**, while the other combination wants to correlate to R–R σ^* but cannot, **28**.
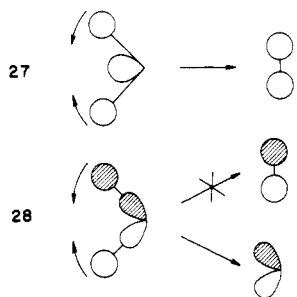

Instead, it correlates to a metal orbital. We are describing in words the avoided crossing so clearly visible at the top of Figure 8 and reproduced schematically in **29** below.

It now becomes clear that the higher the metal yz, the higher the heat of the reductive elimination (left to right in **29**), but also the lower the activation energy for oxidative addition (right to left in **29**). The difference between the square-planar and angular ML_4 fragments lies in the energy of the yz orbital. CpML is perforce related to the angular, and not to the square-planar ML_4, fragment since a cyclopentadienyl must electronically and sterically be the equivalent of three facial and not meridional ligands.

For the ML_4 case we calculate an activation energy for oxidative addition of 0.92 eV. This value can be reduced further if a

(15) Komiya, S.; Albright, T. A.; Hoffmann, R.; Kochi, J. K. *J. Am. Chem. Soc.* **1976**, *98*, 7255–7265. Tatsumi, K.; Hoffmann, R.; Yamamoto, A.; Stille, J. K. *Bull. Chem. Soc. Jpn.* **1981**, *54*, 1857–1867. Hoffmann, R. "Frontiers of Chemistry"; Pergamon Press: Oxford, 1982, 247–263. Pearson, R. G. *Acc. Chem. Res.* **1971**, *4*, 152–160. "Symmetry Rules for Chemical Reactions"; Wiley-Interscience: New York, 1976; pp 286–405. Braterman, P. S.; Cross, R. J. *Chem. Soc. Rev.* **1973**, *1*, 271–294. Åkermark, B.; Johansen, H.; Roos, B.; Wahlgren, U. *J. Am. Chem. Soc.* **1979**, *101*, 5876–5883. Albright, T. A. *Tetrahedron* **1982**, *38*, 1339–1388. Balacz, A. C.; Johnson, K. H.; Whitesides, G. M. *Inorg. Chem.* **1982**, *21*, 2162–2174.
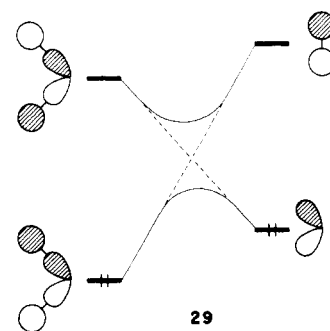
different starting point for the transit is chosen.

Given the importance of a high-lying yz orbital, we can try to think of other coordination geometries that enforce such a circumstance. The d^{10} ML_3 system comes to mind. If it is forced to be pyramidal, as in **30a** or **30b**, then it possesses a high-lying
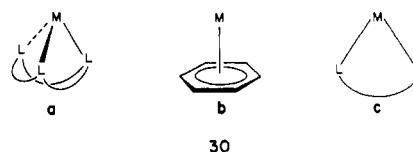
occupied xz, yz pair,[12,16] propitious for a low activation energy for oxidative addition. Our calculations on a $Rh(benzene)^- + CH_4$ model give a barrier of 0.74 eV, starting the transit from an M–H of 1.6 Å. Another system with a high-lying yz level is d^{10} ML_2, **30c**. A calculation on $Rh(CO)_2^-$ addition also gives a low activation energy. We think that such complexes merit investigation as possible C–H activating systems.

Metals and Metal Surfaces

In principle we could build up toward a metal surface slowly by examining a progression of clusters of increasing nuclearity, **31**. As one does this the levels multiply quickly. We strain to
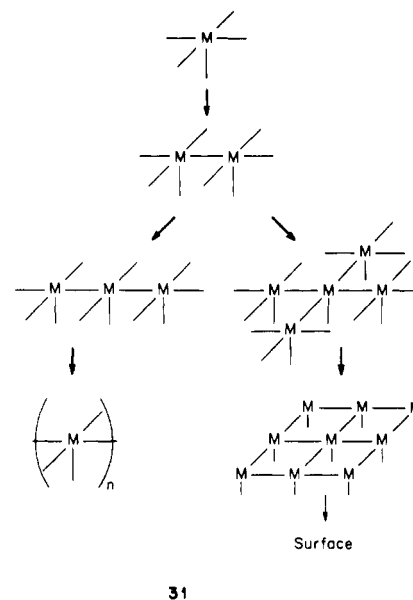
find frontier orbital arguments in which all or most of the responsibility for some basic act of chemical reactivity is placed on one or a subset of frontier molecular orbitals. The perturbation theory-based language obviously remains valid; it just seems that one is doing more work than necessary to trace down the important interactions. There must be a way of thinking about chemical reactivity and structure for infinite extended one-, two-, and

(16) Elian, M.; Chen, M. M. L.; Mingos, D. M. P.; Hoffmann, R. *J. Am. Chem. Soc.* **1976**, *98*, 1148–1155.
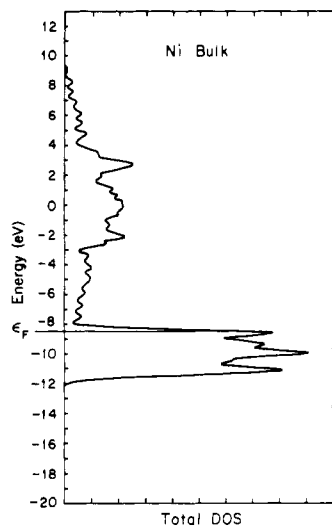
2014 *J. Am. Chem. Soc., Vol. 106, No. 7, 1984*

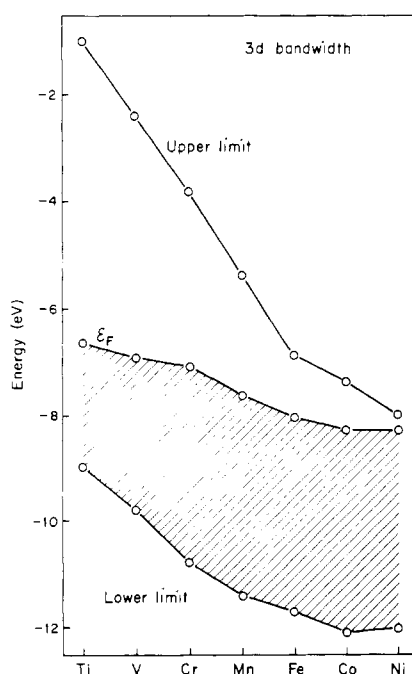*Saillard and Hoffmann*

Figure 9. Density of states of bulk Ni.

Figure 10. 3d bandwidth and position of the Fermi level, as computed by the extended Hückel method, for the first transition series.

Figure 11. Crystal orbital overlap population (COOP) curve for bulk Ni.

three-dimensional materials which deals from the beginning in the properties of bunches of levels and not discrete levels.

Such ways of thinking exist, of necessity cast in the language of solid-state physics.[17] That language is not too difficult to learn, for in fact most of the concepts, though bearing different names, have a one-to-one correspondence with constructs familiar in theoretical chemistry. So instead of levels of different point group symmetry, one has bands of levels distinguished by a translational symmetry label which happens to be a vector in reciprocal space, in k space. The Fermi level is the HOMO, etc. The key to thinking about groups of levels is the density of states, DOS(E), the relative number of states in a given energy interval.

A typical density of states curve for bulk Ni, calculated by the same extended Hückel method as we use for complexes, is shown in Figure 9. Note the "d band", largely metal 3d, between −8 and −12 eV. Above it is a broad s and p band, the bottom of which penetrates substantially into the d band. In fact, at the Fermi

level the populations of the various levels are as follows: $d^{9.15} s^{0.62} p^{0.23}$. Thus, the s-band is one-third filled.[18]

The bulk Ni density of states is characteristic of the rest of the transition series. In Figure 10 we show the d band width and the Fermi level across the first transition series. The Fermi level falls slowly across the transition series. Its calculated value exceeds the observed work function of the metal by ~ 3 eV, which is a typical error of the extended Hückel procedure.

In our discussion of the bonding of molecules to surfaces we have found useful a measure of bonding common in theoretical chemistry, but not often utilized in solid-state physics. This is the Mulliken overlap population between two atoms. In thinking about extended structures it is necessary to think about groups of levels, so the relevant quantity is the overlap population weighted density of states, i.e., the relative number of levels in a given energy interval weighted by the contribution these levels make to the overlap population for a specified bond.[21] We have called these curves COOP curves (for Crystal Orbital Overlap Population). Their integral up to a specified Fermi level is the total overlap population for the given electron count.

In preparation for our use of COOP curves let us show one for Ni–Ni bonding in bulk Ni, Figure 11. The bottom of the d band is metal–metal bonding and the top metal–metal antibonding. Similarly for the s, p band. This is all as expected. The total Ni–Ni overlap population is 0.107 at the Fermi level.

We now move to the Ni surface. The one we have chosen is (111), a closely packed surface. To take full advantage of translational periodicity we must in fact take a film or slab of finite thickness, a typical tactic in solid-state theoretical approaches to surfaces. The thickness of the film should be such as to ensure that it approximates a real surface, yet also the thickness must be kept small for reasons of computational economy. Appendix II details our studies of films varying in thickness from a monolayer to five layers and how we settled on three or four layers as a reasonable approximation to a surface. We have used a four-layer

(17) Ashcroft, N. W.; Mermin, N. D. "Solid State Physics"; Saunders: Philadelphia, 1976. Kittel, C. "Introduction to Solid State Physics"; J. Wiley and Sons, Inc.: New York, 1976. Wannier, G. H. "Elements of Solid State Theory"; Cambridge University Press: New York, 1966.
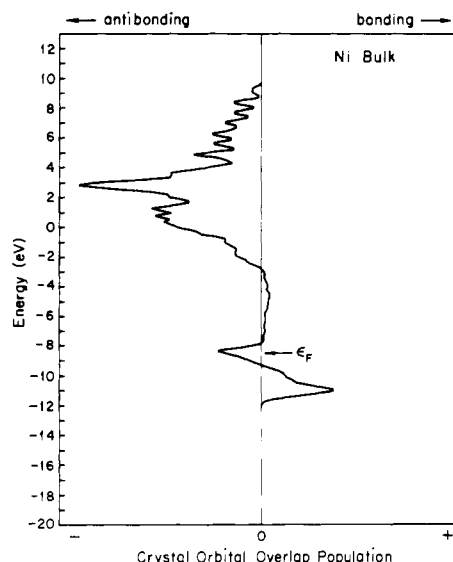
(18) A typical contemporary calculation on bulk Ni, using a method much better than ours, may be found in Wang and Callasay, Wang, C, S.; Callasay, J. *Phys. Rev. B* **1977**, *15*, 298–306. There are some noticeable differences between our band structure and this one, in that in our calculation the DOS in the d band is more uniformly distributed, less peaked.

(19) For an important early extended Hückel calculation of bulk Ni and the (111) surface, see: Fassaert, D. J. M.; van der Avoird, A. *Surf. Sci.* **1976**, *55*, 291–312.

(20) For calculations on the distribution of electrons in the bulk and on the surface, see: Dejonquères, M. C.; Cyrot-Lackmann, F. *J. Chem. Phys.* **1976**, *64*, 3707–3715; Kahn, O.; Salem, L., "Proceedings, Sixth International Congress on Catalysis"; The Chemical Society, London, 1976; Vol. 1, p 101.

(21) Hughbanks, T.; Hoffmann, R. *J. Am. Chem. Soc.* **1983**, *105*, 1150–1162. Wijeyesekera, S.; Hoffmann, R., to be published.
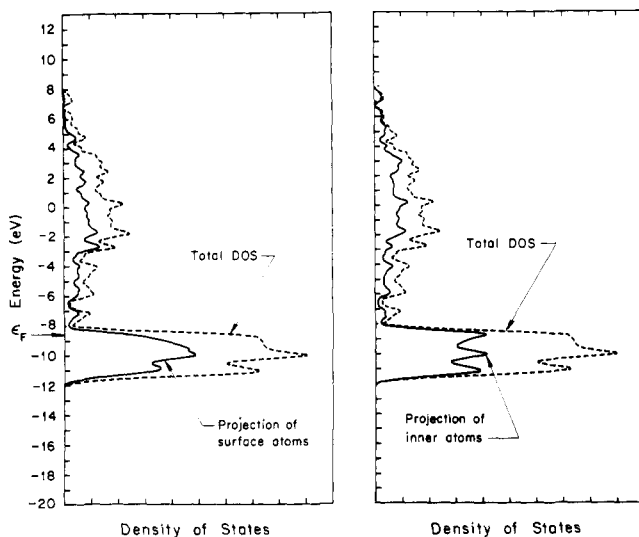
Figure 12. Those parts of the total density of states of a four-layer Ni(111) slab which are on the surface and inner layers. The dashed line is the total density of states.

film in our studies of H_2 chemisorption and a three-layer film for CH_4 activation. The four-layer film is shown schematically in **32**.
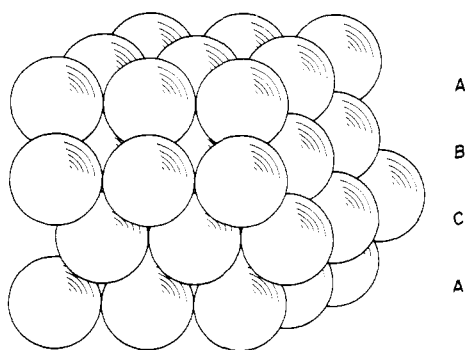

32

The four-layer film has two identical surface-like layers and two identical inner or bulk-like layers. Figure 12 shows the total density of states and its projection or partition among the surface and inner layers. Note that the states in the surface layer have somewhat less dispersion, i.e., form narrower bands. This is true for both the d and the s, p band. The reason for this is simply that the surface atoms have fewer nearest neighbors (9) compared to the inner atoms (12). The number of nearest neighbors affects the number of interactions or overlap available to an atom, and it is the overlap which eventually controls the bandwidth.

This trivial argument, summarized very schematically in **33**, has a nontrivial consequence. If we plot for a given band structure, say that of Ni, the relative number of electrons as one proceeds to fill the band, it is clear that the "bulk"-like layer will fill first. The bulk will be negative relative to the surface. Then at about half-filling the two layers, bulk and surface, will be equally filled. As we fill past this point the surface will become negative. The schematic plot of relative electron distribution as a function of electron count is shown in **34**, and it is supported by our computations.

In reality, as one moves across the transition series to provide the variation in electron count, the average energy of a d electron, i.e., the center of gravity of the bands in **33**, varies as well. The general lines of the argument remain—*at the right side of the transition series surfaces should be negative relative to the bulk, at the left side of the transition series surfaces should be positive.* For the specific case of our four-layer Ni(111) slab the surface atoms each carry a charge of −0.16, while the inner atoms are +0.16.[7,22]
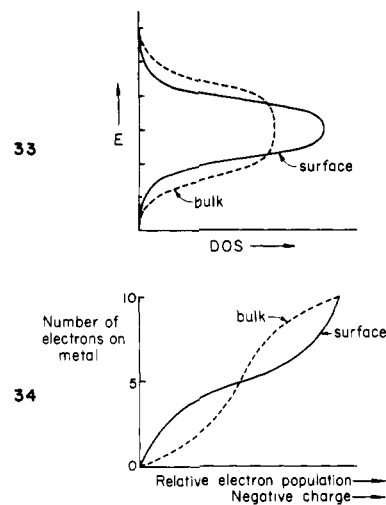

The above-mentioned crossover in the behavior of the electron density at the surface as a function of electron count has been discussed by others prior to us.[7,23] The reader is referred to the excellent papers of Shustorovich[7] for a general development of the subject.

We are now ready to bring H_2 onto the surface.

H_2 on Ni(111)

We cover both sides of the four-layer model film of Ni with a monolayer of H_2, as shown schematically in **35**. There is one
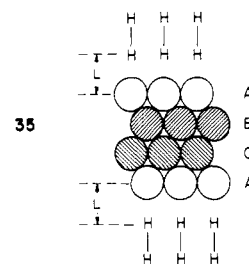

H_2 per surface Ni, i.e., a total slab stoichiometry of $[Ni_4H_4]_\infty$. Each H_2 is "on top" or "perpendicular", above a surface Ni atom.[24] The H–H distance is frozen at 0.74 Å, and the nearest H⋯Ni distance is varied, L. We are studying here as closely analogous a situation as possible to the perpendicular approach of H_2 to a discrete ML_n complex.

The total density of states for L = 3.0, 2.5, 2.0 Å is shown in Figure 13. At 3.0-Å separation we would expect little interaction

(22) For other calculations on the Ni(111) surface, see: (a) Dempsey, D. G.; Grise, W. R.; Kleinman, L. *Phys. Rev. B* **1978**, *18*, 1550–1553. These computations obtain less of a charge shift between surface and inner layers than we do. Among the numerous calculations of surfaces we refer the reader to the following: (b) Arlinghaus, F. J.; Gay, J. G.; Smith, J. R. *Phys. Rev. B* **1980**, *21*, 2055–2059. Gay, J. G.; Smith, J. R.; Arlinghaus, F. J. *Phys. Rev. Lett.* **1979**, *42*, 332–335. Smith, J. R.; Gay, J. G.; Arlinghaus, F. J. *Phys. Rev. B* **1980**, *21*, 2201–2221. (c) Bisi, O.; Calandra, C. *Surf. Sci.* **1979**, *83*, 83–92. (d) Feibelman, P. J.; Appelbaum, J. A.; Hamann, D. R. *Phys. Rev. B* **1979**, *20*, 1433–1443. Appelbaum, J. A.; Hamann, D. R. *Solid State Commun.* **1978**, *27*, 881–883. (e) Fulde, P.; Luther, A.; Watson, R. F. *Phys. Rev. B* **1973**, *8*, 440–452. (f) Dempsey, D. G.; Kleinman, L. *Phys. Rev. B* **1977**, *16*, 5356–5366. (g) Louie, S. G. *Phys. Rev. Lett.* **1978**, *40*, 1525–1528. Experimental studies on the relative electron density of surface and inner atoms include: (h) Citrin, P. H.; Wertheim, G. K.; Bayer, Y. *Phys. Rev. Lett.* **1978**, *41*, 1425–1428. (i) Duc, Tran Minh; Guillot, C.; Lassailly, Y.; Lecante, J.; Jugnet, Y.; Vedrine, J. C. *Phys. Rev. Lett.* **1979**, *43*, 789–792. (j) Van der Veen, J. F.; Himpsel, F. J.; Eastman, D. E. *Phys. Rev. Lett.* **1980**, *44*, 189–198.

(23) See also: (a) Feibelman, P. J.; Hamann, D. R. *Solid State Commun.* **1979**, *31*, 413–416. (b) Desjonqueres, M. C.; Spanjaard, D.; Lassailly, Y.; Guillot, C. *Ibid.* **1980**, *34*, 807–810.

(24) $H_2 \cdots H_2$ interactions are dropped here, but they are anyway small at the intermolecular H⋯H contact of 2.49 Å. When we eventually do CH_4 on the same surface, we will not drop $CH_4 \cdots CH_4$ interactions.
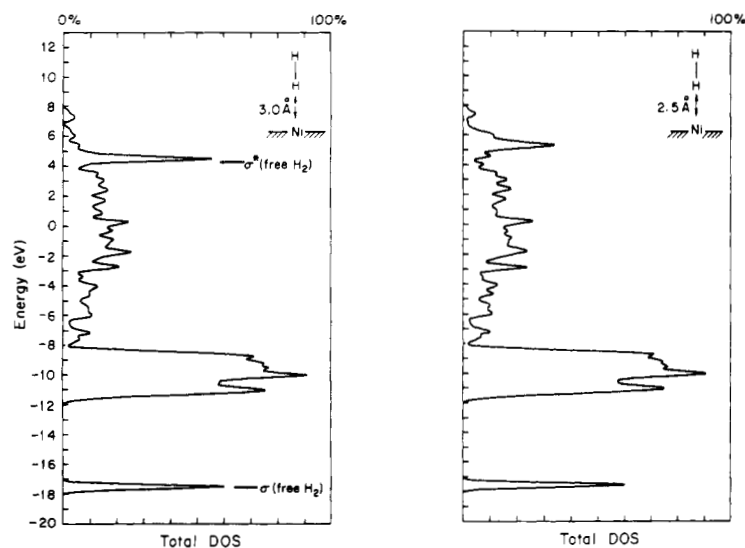
Figure 13. The total density of states for H_2 approaching a four-layer Ni(111) slab at L = 3.0, 2.5, 2.0 Å. The positions of free H_2 σ and σ^* levels are marked on the L = 3.0 Å plot.
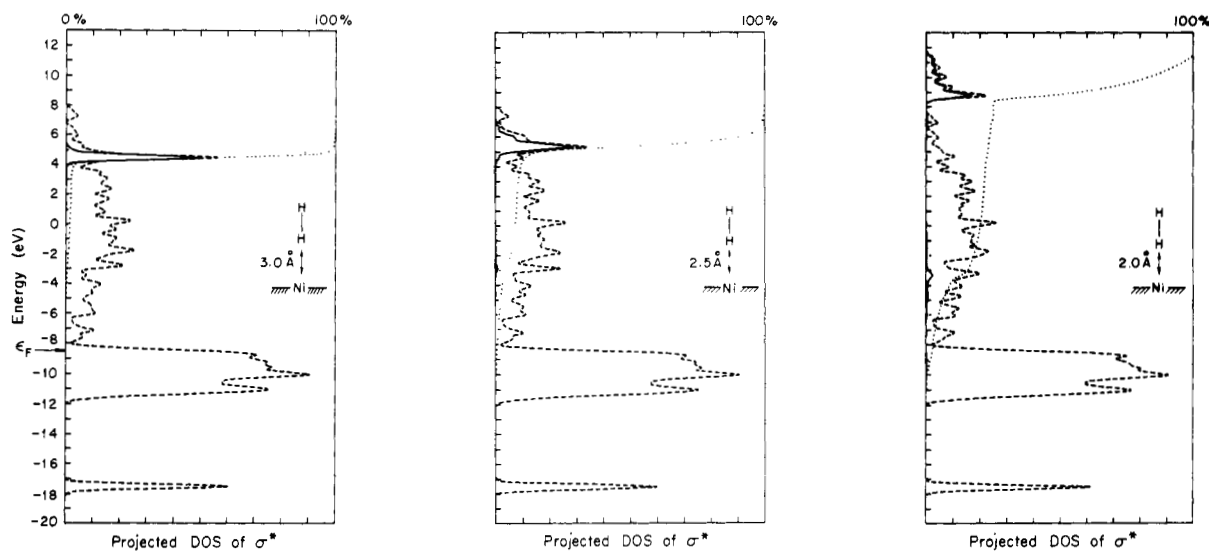
Figure 14. The part of the total DOS (dashed line) which is in the H_2 σ^* (solid line) at various approach distances to a Ni(111) surface. The dotted line is the integrated density in σ^* and refers to the top scale.

between substrate and surface, and indeed what we see is two sharp bands for the monolayers of H_2 σ and σ^*, superimposed on the film band structure. Note, however, even here the slight destabilization of the σ^* band relative to the free molecule value. As the H_2 approaches the surface the σ orbital band retains its identity, persisting in its inefficient interaction with the surface. σ_u^*, on the other hand, begins to break up.
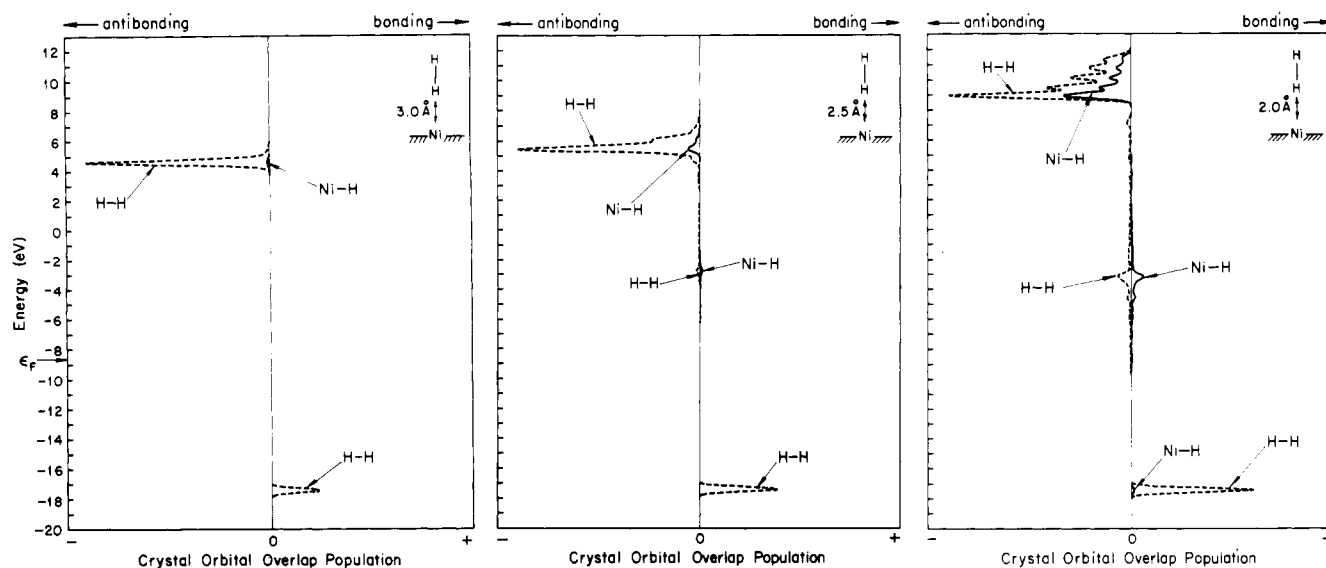
The projections of the density of states on σ_u^* (i.e., the fraction of the DOS that is σ_u^*) of Figure 14 clearly show the strong interaction of σ_u^* with the s, p and d bands. At L = 2.0 Å some fraction of σ^* (2%) has been mixed into the s, p band, especially around -3 to -5 eV. Seventy-five percent of the σ^* is pushed up to high energy, >8 eV. What is happening here is a typical two-level interaction, **36**, except that it is now distributed over the myriad of levels of the H_2 σ^* and metal s, p bands.
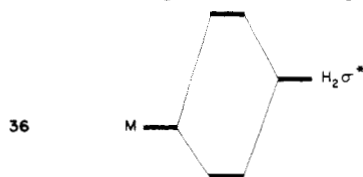
There have been a number of theoretical studies of the interaction of H_2 with transition metal surfaces, modeled either by films

or by clusters.[7,25] We have mentioned earlier the work of Baetzold, Shustorovich, and Muetterties[7] and here refer further to the work of Salem and Leforestier[25a] and of Lundqvist and co-workers.[25b] The former authors stress the importance of interactions with both σ and σ^* of the substrate, much as we will do below. Lundqvist has carried out a thoughtful analysis of metal

(25) (a) Salem, L.; Leforestier, C. *Surf. Sci.* **1979**, *82*, 390–412. (b) Nørskov, J. K.; Houmøller, A.; Johansson, P. K.; Lundqvist, B. I. *Phys. Rev. Lett.* **1981**, *46*, 257–260. Lundqvist, B. I.; Hellsing, B.; Holmström, S.; Nordlander, P.; Persson, M.; Nørskov, J. K. *Int. J. Quantum Chem.* **1983**, *23*, 1083–1090. Lundqvist, B. I.; Gunnarson, O.; Hjelmberg, H.; Nørskov, J. K. *Surf. Sci.* **1979**, *89*, 196–225. Lundqvist, B. I. "Vibrations at Surfaces"; Caudano, R., Gilles, J. M., Lucas, A. A., Eds.; Plenum Publishing Co.: New York, 1982; pp 541–572. Lundqvist, B. I., to be published. (c) Kobayashi, H.; Yoshida, S.; Kato, H.; Fukui, K.; Tamara, K. *Surf. Sci.* **1979**, *79*, 190–205. (d) Andzelm, J. *Surf. Sci.* **1981**, *108*, 561–588. Andzelm, J.; Radzio-Andzelm, E. *Chem. Phys.* **1981**, *61*, 317–323. (e) Charlot, M. F.; Kahn, O. *Surf. Sci.* **1979**, *81*, 90–108. (f) Bohl, M.; Müller, H. *Ibid.* **1983**, *128*, 117–127. (g) Baetzold, R. *Ibid.* **1975**, *51*, 1–13. (h) Fritsche, H. G.; Mertins, G. *Z. Phys. Chem.* **1976**, *257*, 913–928. (i) Anderson, A. B. *J. Am. Chem. Soc.* **1977**, *99*, 696–707. (j) Van Santen, R. A. *Recl. Trav. Chim. Pays-Bas* **1982**, *101*, 121–136. (k) Salem, L.; Elliott, R. *J. Mol. Struct. Theochem.* **1982**, *93*, 75–84. (l) Deuss, H.; van der Avoid, A. *Phys. Rev. B.* **1983**, *8*, 2441. See also ref 18b. (m) These two references contain calculations on CH_3, CH_2, and CH on surfaces: Gavin, R. M.; Reutt, J.; Muetterties, E. L. *Proc. Natl. Acad. Sci. U.S.A.* **1981**, *78*, 3981–3985. Minot, C.; Van Hove, M. A.; Somorjai, G. A. *Surf. Sci.* **1982**, *127*, 441–460.

C-H and H-H Activation in Transition Metal Complexes

J. Am. Chem. Soc., Vol. 106, No. 7, 1984   2017

Figure 15. COOP curves as a function of approach distance of H_2 to a four-layer slab of Ni(111). The solid line is the Ni–H overlap population and the dashed line the H–H overlap population. The lowest peak is in the region of σ of H_2 and the highest where the main density of the σ^* is dispersed.

surface adsorbate interactions. In his model, the H_2 bond breaks because the surface-H_2 resonance corresponding to σ_u^* falls in energy and is filled as H_2 approaches the surface. We do not get such an effect, but perhaps the analogue in the extended Hückel model is the lower group of states induced by σ^* in the s, p band as seen in Figure 14.

We have shown what happens to the energy levels. What about the bonding? We can look at the COOP curves as a function of L (Figure 15). At large L the H–H bonding is picked up as one sweeps through the σ_g level and H–H antibonding (more than the bonding!) as one passes through σ_u^*. As one moves the H_2 in these features persist, but now Ni–H bonding enters. Look at $L = 2.0$ Å. There is a little Ni–H bonding as one sweeps through the H_2 σ bond. Above that, until one enters the main density of σ_u^*, one passes through a region of Ni–H bonding (and mirrored H–H antibonding).

The sign of these bonding interactions is a vital clue to the role of σ and σ^* in the bonding to the surface. There are two extreme possibilities: (a) σ–metal interaction dominant; (b) σ^*–metal mixing predominating. Each possibility has different consequences for M–H and M–M bonding, as we will now show.

Suppose σ–M mixing were dominant. Then in some localized orbital scheme we would get **37**, simple in- and out-of-phase mixings of σ and some appropriate symmetry metal orbital. The resultant COOP curve, when this kind of thinking is extended to a band picture, would have the σ band H–H and M–H bonding, whereas the corresponding metal band is still H–H bonding but M–H antibonding (**38**).

37

38
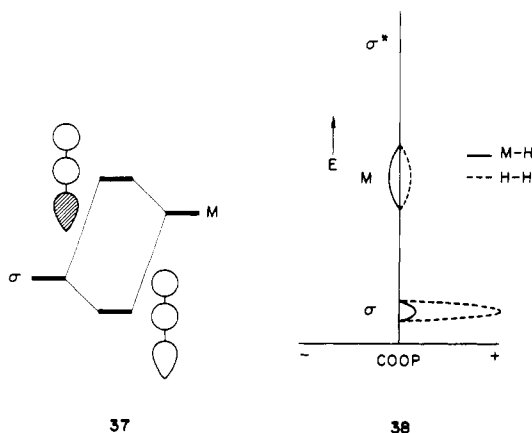
Suppose instead σ^*–M mixing were dominant. Then the localized picture is like **39**, and the expected COOP curve like

40. Now the lower, primarily metal band is M–H bonding but H–H antibonding, through the admixture of σ^*. The σ^* band itself is both H–H and M–H antibonding.


39

40
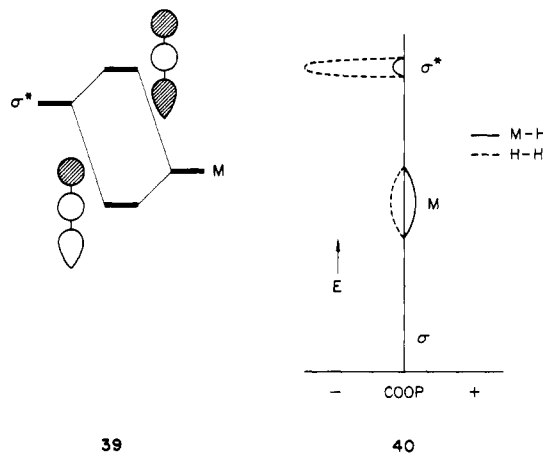
Reality is the superposition of the two effects. There is no question what will dominate in the region of the bands derived from H_2 σ_g and σ_u^*. But in the region of the bands derived from the metal the two models give opposite predictions: if σ mixing were dominant over σ^*, the intermediate region should be H–H bonding and M–H antibonding. The reverse should be true if σ^* mixing were dominant. Figure 15 gives a clear answer: In the intermediate region, in the metal bands, the mixing of metal orbitals is largely in a bonding way with H_2, and H–H bonding is weakened in the same region. Clearly metal surface–hydrogen σ^* mixing is dominant.

Why is this so? There are both energy and overlap reasons. σ_u^* of H_2 lies in the s, p band to begin with. Second, the σ_u^* coefficients are greater, so their overlap with appropriate symmetry surface states is perforce greater than that of σ_g^*.

So far we have looked at the most informative overall picture, independent of electron count. But now it is time to focus our attention on Ni, and what happens below its Fermi level, for its particular electron count.

The overall charge flow and population analysis changes as a function of L are given in Figure 16. Ni–H bonding is turned on as L decreases, and H–H bonding is decreased. This is accomplished by populating σ^* of H_2, with relatively minor depopulation of σ. Note the difference between activation in the discrete complex (σ^* not much populated) and on the metal surface (σ^* reasonably populated). The important role of the σ^* in H–H or C–H bonding has been stressed in a number of previous
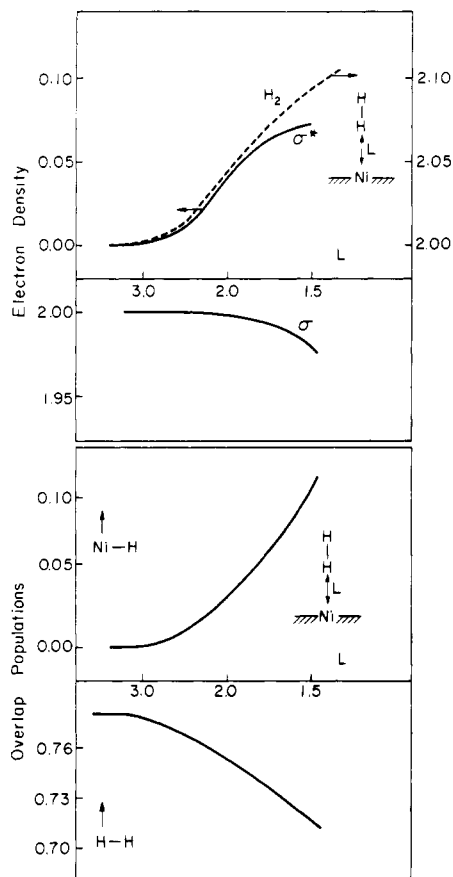
Figure 16. M-H and H-H overlap populations (bottom) and σ, σ^* and total H_2 densities (top) as a function of L, as H_2 approaches the four-layer slab of Ni(111).
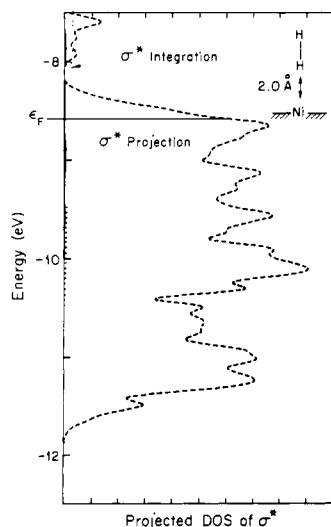
Figure 17. That part of the total DOS (dashed line) which is the H_2 σ^* (solid line hugging the energy axis). This is at $L = 2.0$ Å, and the energy window shows the Ni(111) d block only. The integrated σ^* population is the dotted line.

studies,[7,25] especially those of Baetzold, Shustorovich, and Muetterties.[7]

To see how the bond breaking occurs in detail we must apply a microscope to Figures 13 and 14 and zoom in on the metal d band, -8 to -12 eV. This is where the action takes place. Figure 17 shows the total DOS of the Ni(111) four-layer film with H_2 overlayers, $L = 2.0$ Å, in this smaller energy window. The projection of these states on σ is too small to show up, but that of σ^* is clearly visible. It is the integral of this projection up to the Fermi level which gives the 0.044 population of σ^* that may be read off Figure 16.
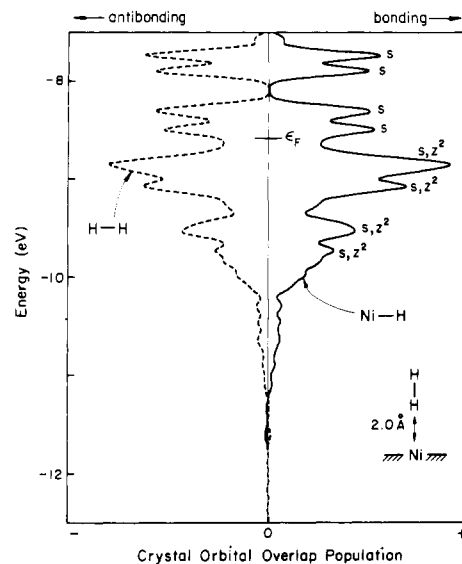
Figure 18. The COOP curve for Ni-H and H-H bonding in the d block region. H_2 here has approached to $L = 2.0$ Å. Those peaks in the COOP curve which pick up maxima in the projected DOS curve of surface s and z^2 are marked accordingly.

So σ^* penetrates the d band and is responsible for M-H bonding. But in more detail how does it do it? We can apply a microscope to Figure 15 and zoom in on the COOP in the d band. This is Figure 18. Please note that the scale on the COOP curves is *not* the same for Figures 18 and 15. The Ni-H and H-H curves mirror each other. Further insight may be obtained by looking at projections of the DOS of the Ni(111) film alone on s, z^2, and xz, yz components of the surface layer, Figure 19. These are the prime orbitals of σ and π local pseudosymmetry with respect to the impacting H_2.

The features in the COOP curve of Figure 18 clearly pick up corresponding features of the DOS of surface s and/or surface z^2. We have marked the most obvious features in the corresponding curves. The picture is chemically consistent. *The surface interacts with the substrate H_2 mainly through H_2 σ_u^* and surface layer s and z^2 orbitals.*

So far we have restricted ourselves to an "on-top", perpendicular approach of H_2 to a Ni surface. Clearly other sites of adsorption and the parallel geometry must be considered. In fact, we studied further five basic geometries, **41-45**. **41** may be described as threefold, perpendicular, **42** as twofold, perpendicular, **43** as on-top, parallel, **44** as on a bond, parallel, and **45** as across a bond, parallel. For each of these we studied a range of metal-H_2 separations.
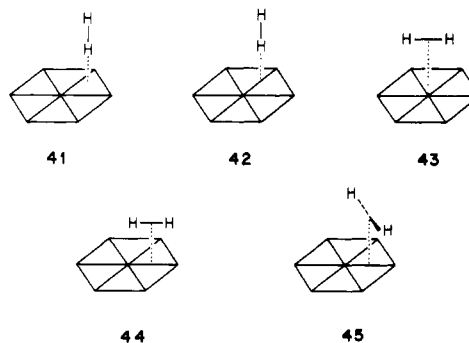
It was mentioned earlier that we cannot trust the extended Hückel calculations for the energetics of bond forming or breaking. One would have liked to be able at least to predict reliably relative sites of adsorption, but unfortunately we cannot do that. *All* of the approach geometries, parallel or perpendicular, give rise to repulsive energy curves. The method overestimates the four-electron repulsive component of the interaction energy. Perhaps one could still hope to argue from the softness or hardness of the repulsion, but we would prefer to abandon the energy criterion
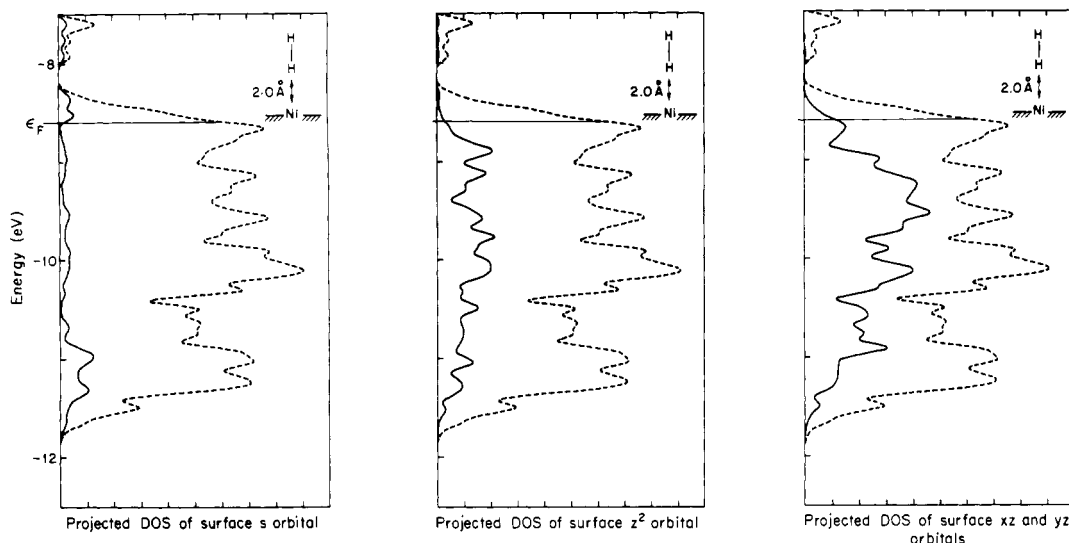
Figure 19. The parts of the total DOS of a four-layer slab model Ni(111) which are in the surface layers s, z^2 and xz, yz orbitals. The total DOS is represented, at a smaller scale, by the dashed line curve.

and focus instead on what we know extended Hückel does reasonably well in molecules—the method gives a reasonable estimate of bonding interactions, especially those dependent on orbital symmetry.

We chose to compare the various approaches of H_2 at a similar Ni–H separation of ~2.0 Å. Table I gives several calculated quantities for the geometries studied: the Fermi level energy, the change in total energy, M–H and H–H overlap populations, H_2 σ and σ^* populations, the *changes* in populations of the surface metal layer (both total and classified according to orbital and symmetry type (s, p_σ, p_π, d_σ, d_π, d_δ)), and the total change in the inner or bulk-like layer. The changes are relative to the free surface, and in every case the convention is that a negative number implies loss of electron density, or an increasing positive charge.

Let us review what happened in the first on-top, perpendicular approach. The Fermi level is raised slightly, the approach is destabilizing or repulsive, M–H forms, and H–H begins to weaken. There is minimal effect on σ, but substantial electron transfer to σ^* of H_2. That electron transfer occurs primarily from the surface layer and in the surface primarily from the s and d_σ ($=z^2$) orbitals. All other effects are small.

Threefold, Perpendicular, 41: In this geometry there is substantial destabilization, yet good M–H bond formation and H–H bond weakening. The COOP curve of Figure 20 shows something new, some features at low energy which indicate interaction with σ in addition to σ^*.

What is happening here is that both H_2 σ and σ^* can interact with surface orbitals which are bonding between all three metals, as shown schematically in **46**. These orbitals are the 3d orbitals
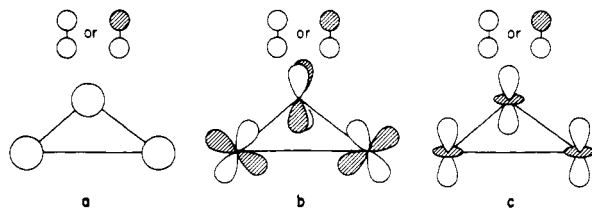

46

at the bottom of the band and most of the s orbitals in the d band, since the latter are the bottom of the s band.[26]

The interaction is strong, because it occurs with three metal atoms instead of one. σ^* still dominates the mixing, but there are signs that σ begins to enter the picture. Note for instance

(26) This way of thinking is related to the "surface amplitude patterns" developed by Minot et al.: Minot, C.; Kahn, O.; Salem, L. *Surf. Sci.* **1980**, *94*, 515–527.
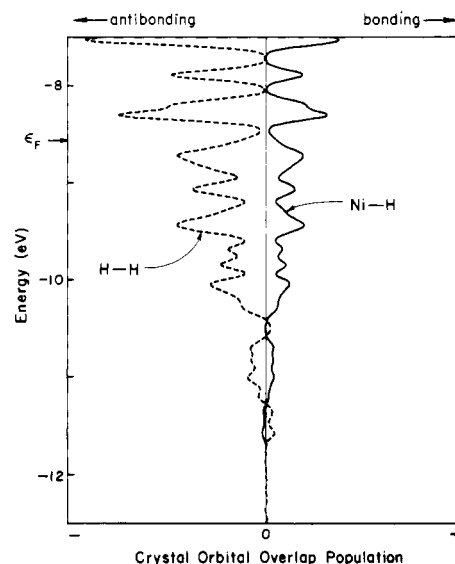

Figure 20. The COOP curve for Ni–H and H–H bonding when H_2 is perpendicular to the surface, on top of a threefold hollow site (geometry **47**).

the destabilization, the result of (overestimated) interactions between the surface and σ. Also the Fermi level rises slightly.

One interesting feature which is the result of the stronger interaction is the polarization of the metal by the adsorbate. H_2 gains 0.065 e, but the surface layer loses -0.121 e. It loses them to H_2, but also to the inner or bulk layer. What is at work here is interaction ④ discussed in an earlier section, a substrate-induced reorganization of electron density. This interaction has also been discussed by Shustorovich.[7] Let us examine this process in some detail.
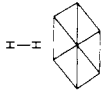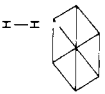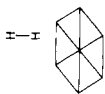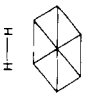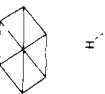
Suppose that there is some distribution of levels in the band such that some levels are more surface-like than bulk-like. This is shown schematically in **47**, where the surface-like levels are
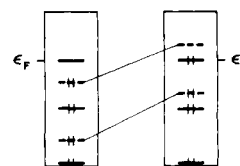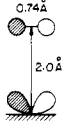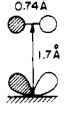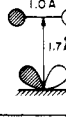

47

marked as dashed lines and the bulk-like levels as solid lines. If

2020   J. Am. Chem. Soc., Vol. 106, No. 7, 1984

Saillard and Hoffmann

Table I. The Consequences of H_2 Approaching Ni(111) in Different Orientations

geometry	overlap populations		H_2 electron densities		Ni surface layer change[b] in electron density (total)	Ni surface layer electron density changes[c]						Ni inner layer change[b] in electron density	ΔE,[d] eV	ϵ_F, eV
	Ni-H[a]	H-H	σ	σ^*		Δs	Δp_σ	Δp_π	Δd_σ	Δd_π	Δd_δ			
surface and H_2 at infinite separation	0	0.782	2.000	0	0	0	0	0	0	0	0	0	0	8.587
	0.034	0.752	1.997	0.044	-0.049	-0.018	-0.004	+0.000	-0.027	+0.001	+0.001	+0.008	0.060	-8.587
	0.053	0.742	1.993	0.072	-0.121	-0.078	-0.009	-0.011	-0.018	-0.014	+0.011	+0.055	0.328	-8.582
	0.047	0.745	1.993	0.065	-0.102	-0.064	-0.009	-0.006	-0.019	-0.011	+0.008	+0.044	0.118	-8.583
	-0.017	0.768	1.985	0.023	-0.114	-0.102	-0.007	+0.004	-0.049	-0.000	+0.038	+0.107	0.452	-8.568
	0.061	0.747	1.987	0.050	-0.180	-0.126	+0.006	-0.018	-0.075	-0.012	+0.045	+0.144	0.434	-8.547
	0.007	0.753	1.979	0.041	-0.203	-0.176	+0.003	-0.021	-0.024	-0.041	+0.058	+0.183	0.750	-8.538

[a] In cases where there is more than one M–H contact, the entry is for all the Ni–H contacts, to one H_2 molecule, summed. [b] Electron density of both surface (or inner) layers, summed, relative to the layer without H_2. Negative Δn means loss of electron density, or positive character. [c] Electron densities of specified orbitals in both surface layers, summed, relative to the same orbitals in the uncovered surface layer. Negative numbers mean electron density is lost. [d] E(geometry) $- E$(separated H_2 and Ni films). Positive ΔE implies destabilization.

Table II. Interactions of Several Geometries in the On-Top, Parallel Approach of H_2

	$\langle xz|\sigma_u{}^* \rangle$	overlap populations		charges	
		M–H	H–H	σ	σ^*
	0.072	−0.017	0.768	1.985	0.023
	0.125	0.048	0.732	1.974	0.042
	0.130	0.186	0.490	1.934	0.211

the dominant interaction, as far as energy is concerned, is repulsive (in our case with H_2 σ), then surface-like levels will be pushed up more, some above the Fermi level. The surface layer will be depopulated relative to the bulk. And within the surface those levels primarily involved in interaction (s, d_σ, d_π) will be depopulated relative to those not participating in interaction (for example d_δ).

In the case at hand we see clearly the surface-to-bulk electron shift and the increased population of the d_δ, in-plane orbital set. This, in turn, will cause some decrease in metal–metal bonding in the surface because the newly filled d_δ levels are metal–metal antibonding.

Twofold, Perpendicular, 42: As might have been expected, the results for this geometry are intermediate between the on-top and threefold sites.

On-Top, Parallel, 43: The gross indicators of this geometry of approach are disappointing—M–H is not even slightly bonding, and given how good σ^*–M interaction was in the discrete complex it is startling to see so little population of H_2 σ^*. How can this be?

The solid-state case of course is much more complicated than the discrete molecular one. For $L_5M–H_2$ in a parallel geometry the H_2 σ orbital was not allowed, by symmetry, to interact with the same t_{2g} orbital that gained so much when it mixed σ^* into itself. In the extended solid both σ and σ^* of H_2 mix with the metal t_{2g} orbitals everywhere in the interior of the Brillouin zone. The surface analogue of the π bonding t_{2g} orbital is subjected to both stabilizing and destabilizing forces.

Informative in this respect is the COOP curve of Figure 21, left. The peaks of negative Ni–H (and positive H–H) correspond to peaks in the DOS of s and z^2. It is clear that repulsive interactions with H_2 σ dominate the interaction.

But there is a glimmer of hope. In the lower region of the band the peaks of negative H–H overlap population (minima in the Ni–H overlap population) correspond to peaks in the projected DOS of xz (Figure 19). If the $\sigma^*–xz$ overlap could be increased perhaps this interaction could be magnified. This can be accomplished by bringing H_2 closer to the surface, **48**, and by


48 **49**
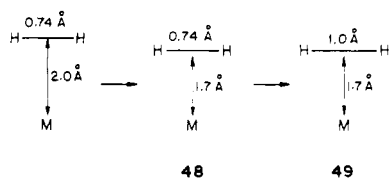
stretching the H_2 bond, **49**. Some fragment overlaps which demonstrate this are shown in Table II, which also gives population changes as a result of these distance changes.

Bringing H_2 closer to the metal (**48**) increases the $\sigma^*–xz$ overlap greatly. M–H becomes bonding and σ^* significantly populated. The COOP curve shows increasing improvement in M–H_2 bonding and a growing role for xz. Stretching H_2 makes for still stronger M–H bonding and, of course, substantial population of σ^*. The $\sigma^*–xz$ interaction dominates the COOP curve.

An interesting feature of the COOP curves is that they indicate stronger M–H_2 bonding for a total electron count of 9, i.e., one less than Ni, for Co. It is this kind of selective catalytic information that we hope to obtain in future studies in this area.

Clearly we have a dissociative process at work. But in the early stages of the reaction it is repulsive and needs some activation energy. Another parallel approach seems more promising.

On-a-Bond, Parallel, 44: There is good bonding overall, though repulsive contributions still dominate. Each H_2 interacts significantly with two metal atoms. Characteristic σ mixing, shown in **50**, is with z^2 and xz in the lower part of the d band and with

50 **51**
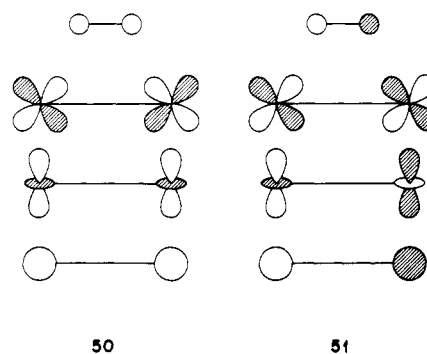
s throughout the band. There is much polarization of the metal and electron reorganization within the surface. The H_2 σ^* orbital interacts predominantly with xz and z^2 combinations of type **51**, in the upper part of the band. The resultant population of σ^* is good, and the Ni–H overlap population is the largest in Table I. Once again a somewhat lower electron count will give better M–H bonding.

The alternative **across-a-bond, parallel** geometry, **45**, shows no special features, though its bonding interactions grow if H–H is stretched.

To summarize: We cannot compute a potential energy surface, but with some detective work through the projected DOS and COOP curves and populations we can trace the origins of the various bonding trends. A significant aspect of this section is our finding of optimum M–H bonding for a parallel geometry in which H_2 is lying over a bond, **44** or **52**. This kind of two-metal-assisted cleavage of H_2 is not possible in a discrete mononuclear complex.


52
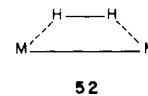
The important underlying theme of this analysis is that the interaction of H_2 with a metal surface is qualitatively no different from the similar interaction with the metal center of a discrete molecule. There are important differences in the pacing of involvement of the H_2 σ and σ^* (σ^* is more important in the surface case). But the fundamental aspects of the reaction, which we discussed in the introduction, remain. There is transfer of electrons from H_2 σ to H_2 σ^*. As a result, the H–H bond breaks and M–H bonds form.

Methane on Ni(111)

A 1:1 coverage of a close-packed metal surface by methane is not possible, no matter what the approach geometry. The reason for this is excessive steric hindrance between the methanes. We went to a coverage of a third, using the unit cell shown in a solid line in **53**, instead of the 1:1 coverage originally used, dashed line. The reduced coverage is $(\sqrt{3} \times \sqrt{3})R(30°)$. The larger unit cell thus brought about forced us to a three-layer film in place of the four-layer one we had used previously. We also economized by covering only one side of the film.
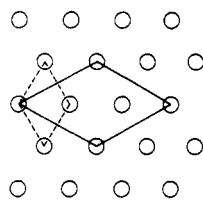
53

Several geometries are feasible, **54–58** among them. The methane molecules, fixed tetrahedral with C–H $\approx$ 1.1 Å,[27] were placed so that all the closest Ni–H contacts were 2.0 Å. The

54, 1 H on top   **55, 1 H three fold**   **56, 3H**

57, 2H along bond   **58, 2H across bond**
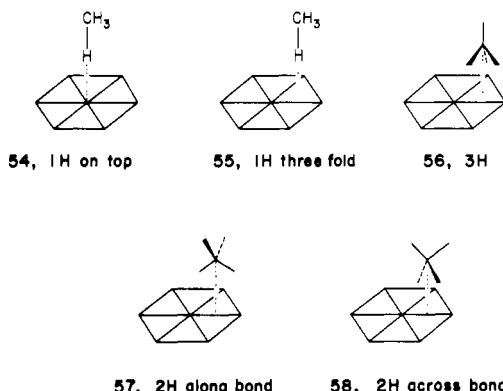
various approaches are labeled by the number of hydrogens directed toward the surface and by a geometrical descriptor. Some calculated quantities, paralleling those we found useful to analyze for adsorbed H_2, are given in Table III. Among the three t_2 (σ) orbitals of CH_4, those which are interacting preponderantly with the surface are the ones bearing the largest coefficients on the interacting hydrogen(s). These orbitals are shown in **59**.[26] Notice

1 H, on top   **1 H, three fold**   **3 H**

2 H, along bond   **2 H, across bond**
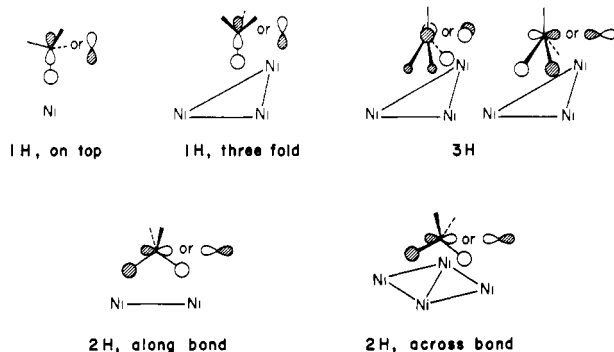
59

that in all cases, σ and σ^* have the same phase relationship on the interacting hydrogen(s) and consequently will interact with the same surface orbitals. The 1H geometries, on-top or over a threefold site, are remarkably similar to their H_2 counterparts. There is repulsion, M–H bonding, C–H bond weakening, transfer of electrons from methane σ and into σ^*, loss of electrons from surface s, and d_σ, substantial polarization of the surface. In general there is more mixing with methane C–H σ orbitals. This was expected, for it will be recalled that the CH_4 t_2 is $\sim$2 eV above H_2 σ_g, and thus closer in energy to the metal d block. The stronger interaction with methane σ manifests itself in the greater, relative to H_2, depopulation of σ, and the greater reorganization in the metal, see the population shift to the inner layer and d_δ.

Like H_2, **54**, CH_4 in the threefold site, gives more surface-adsorbate bonding than **53** because of its larger number of Ni···H contacts.

---

(27) Actually the C–H bonds pointing toward the metal were taken as 1.10 Å, so as to simplify the analysis. The other C–H bonds were 1.09 Å.

The 3H and 2H geometries, which have several of these contacts, are excellent for Ni–H bond formation. In **56** and **57**, since the H atoms are close to on-top positions, the interacting surface states are s and z^2. **58** gives the larger Ni–H overlap population, in this geometry s surface orbitals are involved but also interactions of type **60** are engendered between σ^* and a piece of the yz band. The geometrical match and overlap are excellent. The culmination of double C–H bond breaking in this geometry would be the formation of surface hydride and methylene.

Geometries in which *one* Ni atom is in contact with 2 or 3 H atoms have also been studied. In both cases negative Ni–CH₄ overlap populations are found, resulting from strong repulsive interactions of type ③. These occur via the H atoms and also through the C atom which in these geometries is not far from the Ni atom.

"front"   "side"
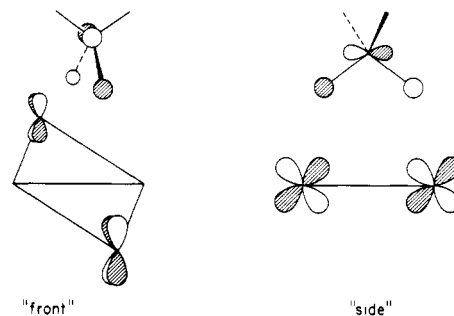
60

We have mentioned earlier the important recent study of Baetzold[7] on the interaction of hydrocarbons with transition metal films. That work is very much in the same spirit as ours. We are in agreement in the direction of charge transfer between methane and the surface and the importance of the σ^* orbitals. There is some disagreement between our respective calculations on the preference given to different geometries of approach.

Returning to general considerations, we think that it is interesting that the overlap population corresponding to *one* interacting hydrogen in **58** is about equal to the Ni–H overlap population in **54** and lower than the one of **55**. The C–H overlap population in these three geometries is also about the same. This leads us to think that for cyclic or chain alkanes chemisorption may proceed by a variety of surface–H contacts, the major criterion of stability being the largest possible number of H atoms in contact with the surface that can be produced by matching of the surface and alkane geometries. Recent studies of cyclohexane on Ru(001), where contacts of the kind of **54** are suggested,[6f,m] support this idea.

H_2 and CH_4 on Titanium

The (001) surface of Ti hcp exhibits hexagonal packing very similar to Ni(111): the stacking is of the type ABAB for Ti(001) and ABCABC for Ni(111). The main difference between the two surfaces can be understood from Figure 10: Ni and Ti are at each end of a monotonic series. The Fermi level of Ti is $\sim$2 eV higher in energy than the one of Ni. Consequently interactions of type ②, metal acting as donor relative to σ^* orbitals, are expected to be greater with Ti. This is also reinforced by a better overlap of σ^* orbital with surface orbitals, due to the diffuseness of Ti atomic orbitals. On the other hand, the bottom of the Ti d band is $\sim$3 eV higher in energy than the one of Ni, and consequently repulsions of type ③ are smaller with Ti.
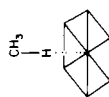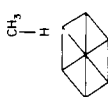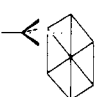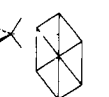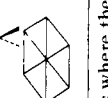
For H_2 dissociation the same geometries (except for **41**) as for H_2 on Ni(111) have been studied; the main calculated quantities are summarized in Table IV.

Qualitatively, there is no big difference between the bonding of H_2 on Ti(001) and on Ni(111). However, except for H_2 on top of a metal atom, considerably larger metal–H overlap populations are obtained, associated with small H–H overlap populations.[28] Clearly, Ti is much more dissociative than Ni. The

---

(28) This trend has also been noted and explained by Baetzold in ref 7.

C–H and H–H Activation in Transition Metal Complexes

J. Am. Chem. Soc., Vol. 106, No. 7, 1984 2023

Table III. The Consequences of Approaching CH_4 to Ni(111) in Different Orientations

geometry	overlap populations Ni-H[a]	overlap populations C-H[b]	CH_4 electron densities σ	CH_4 electron densities σ*	Ni surface layer change in electron density (total)[c]	electron density changes in Ni surface layer[d] Δs	Δp_σ	Δp_π	Δd_σ	Δd_π	Δd_δ	Ni inner layer change in electron density	ΔE,[e] eV	ε_F, eV
surface and CH_4 at infinite separation	0		8.0	0	0	0	0	0	0	0	0	0	0	-8.587
	0.037	0.763	7.984	0.036	-0.057	-0.040	-0.003	-0.001	-0.046	+0.004	+0.020	+0.037	0.154	-8.573
	0.050	0.760	7.974	0.055	-0.081	-0.203	-0.016	-0.021	-0.061	+0.012	+0.109	+0.152	0.559	-8.558
	0.067	0.773	7.961	0.062	-0.263	-0.263	-0.014	-0.019	-0.136	+0.034	+0.136	+0.240	0.882	-8.555
	0.057	0.769	7.971	0.049	-0.168	-0.145	-0.009	-0.009	-0.108	+0.022	+0.074	+0.148	0.480	-8.559
	0.078	0.762	7.959	0.093	-0.450	-0.098	+0.003	-0.010	-0.011	-0.028	+0.062	+0.398	1.140	-8.558

[a] In cases where there is more than one Ni–H contact, the entry is for all the Ni–H contacts, toward one CH_4 molecule, summed. [b] Average of bonds pointing toward the surface. [c] Electron density of the surface layer next to CH_4, relative to CH₄, relative to the same layer without CH_4. [d] Electron densities of specified orbitals in the surface layer atoms in contact with CH_4, relative to those in the uncovered layer. [e] E(geometry) − E(separated CH_4 and Ni films).

Table IV. Titanium(001)-H_2 Interactions

structure	overlap populations		H_2 electron densities	
	Ti-H[a]	H-H	σ	σ^*
	0.026	0.755	1.998	0.041
	0.112	0.682	1.988	0.120
	0.068	0.695	1.993	0.102
	0.420	0.603	1.990	0.211
	0.238	0.590	1.986	0.231

[a] In cases where there is more than one Ti-H contact, the entry is for all of the Ti-H contacts to one H_2 molecule, summed.

Table V. Titanium(001)-CH_4 Interactions

structure	overlap populations		CH_4 electron densities	
	Ti-H[a]	C-H[b]	σ	σ^*
	0.045	0.770	7.983	0.024
	0.115	0.724	7.997	0.124
	0.167	0.767	7.960	0.089
	0.108	0.767	7.975	0.057
	0.157	0.748	7.998	0.169

[a] In cases where there is more than one Ti-H contact, the entry is for all of the Ti-H contacts toward one CH_4 molecule, summed.
[b] Average of bonds pointing toward the surface.

geometry of type **44** is still the best candidate for a low-energy dissociative process.

An approach configuration of type **45** gives much more metal-H bonding with the Ti(001) surface. This is also a consequence of the diffuseness of titanium atomic orbitals: The interaction of σ^* with the nearest metal atom is of δ type, and this interaction is weak on Ni(111) but larger on Ti(001), due to better overlap with diffuse yz Ti atomic orbitals. In addition, the interaction with the second nearest metal (situated for both surfaces at $\sim$ 2.4-2.5 Å) is negligible on Ni(111) but important on Ti(001).

Table VI. Extended Hückel Parameters Used in Molecular Calculations

| orbital	H_{ii}, eV	ζ_1	ζ_2	$C_1{}^a$	$C_2{}^a$
Cr 4s	−8.66	1.70			
4p	−5.24	1.70			
3d	−11.20	4.95	1.60	0.4876	0.7205
Fe 4s	−9.10	1.90			
4p	−5.32	1.90			
3d	−12.60	5.35	2.00	0.5505	0.6260
Rh 5s	−8.09	2.135			
5p	−4.57	2.100			
4d	−12.50	4.29	1.97	0.5807	0.5685
P 3s	−18.60	1.60			
3p	−14.00	1.60			
Cl 3s	−30.00	2.033			
3p	−15.00	2.033			
C 2s	−21.40	1.625			
2p	−11.40	1.625			
O 2s	−32.30	2.275			
2p	−14.80	2.275			
H 1s	−13.60	1.30			

[a] Contraction coefficients used in the double-ζ expansion.

**Table VII.** Extended Hückel Parameters Used in Metal Bulk and Surface Calculations

orbital	H_{ii}, eV	ζ_1	ζ_2	$C_1{}^a$	$C_2{}^a$
Ti 4s	−6.3	1.50			
4p	−3.2	1.50			
3d	−5.9	4.55	1.40	0.4206	0.7839
V 4s	−6.7	1.60			
4p	−3.4	1.60			
3d	−6.7	4.75	1.50	0.4560	0.7520
Cr 4s	−7.3	1.70			
4p	−3.6	1.70			
3d	−7.9	4.95	1.60	0.4876	0.7205
Mn 4s	−7.5	1.80			
4p	−3.8	1.80			
3d	−8.7	5.15	1.70	0.5140	0.6930
Fe 4s	−7.6	1.90			
4p	−3.8	1.90			
3d	−9.2	5.35	1.80	0.5366	0.6678
Co 4s	−7.8	2.00			
4p	−3.8	2.00			
3d	−9.7	5.55	1.90	0.5550	0.6678
Ni 4s	−7.8	2.10			
4p	−3.7	2.10			
3d	−9.9	5.75	2.00	0.5683	0.6292

[a] Contraction coefficients used in double-ζ expansion.

The total resulting interaction is shown in projection in **61**. It involves the bottom of the yz band.

61
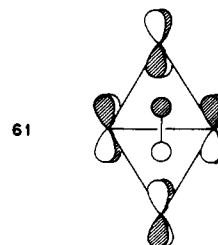
Another typical feature of Ti(001) is that for some geometries, namely **43** and **44**, the bulk layer is depopulated. This is the consequence of another variant of interaction ④, the "reverse" of **47**, shown in **62**. Some empty surface states situated close
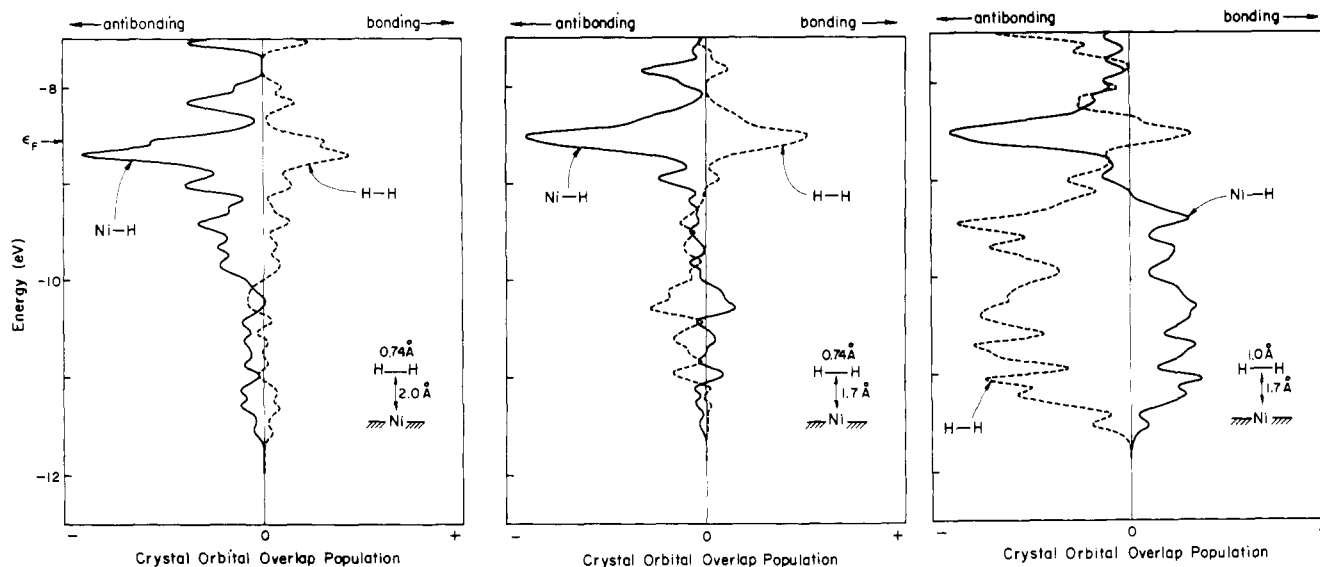

62
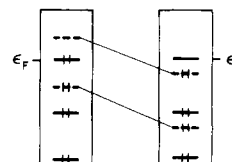
Figure 21. Evolution of the COOP curve for Ni–H and H–H bonding when H_2 is in the on-top, parallel geometry **43** as the molecule approaches the surface and the H–H bond is stretched.

Table VIII. The Effect of Slab Thickness on Models for Ni(111)

| no. of layers | layer no. | electron densities | | | | overlap populations between neighbors | | ϵ_F, eV |
		total	s	p	d	on surface	inside slab (av)	
1	1	10.00	0.66	0.14	9.20	0.171		−9.04
2	1	10.00	0.58	0.19	9.23	0.131	0.109	−8.71
3	1 (surface)	10.10	0.63	0.20	9.27	0.134	0.112	−8.59
	2 (middle)	9.79	0.60	0.24	8.95			
4	1 (surface)	10.16	0.63	0.20	9.33	0.132	0.110	−8.56
	2 (middle)	9.84	0.61	0.24	9.00			
5	1 (surface)	10.21	0.63	0.20	9.38	0.130	0.110	−8.56
	2	9.89	0.61	0.24	9.04			
	3 (middle)	9.80	0.62	0.23	8.95			
3 D bulk Ni		10.00	0.62	0.24	9.15	0.107		−8.47

to the Fermi level are, by interaction with σ^*, pushed down below the Fermi level and become populated, taking their electrons from noninteracting (bulk and surface d_δ) filled levels situated near the Fermi energy.

For methane on Ti the results summarized in Table V are not qualitatively very different from those concerning CH_4 on Ni(111). Geometries **56** and **58** give the strongest Ni–H bonds. As for H_2, the metal–hydrogen overlap population is larger for Ti(001) than for Ni(111) and the H–C overlap population lower. One may expect more dissociative chemisorption of saturated substrates on the surface of metals situated on the left side of the periodic table.

Concluding Comments

The problems that the extended Hückel method has with bond distances have not deterred us from seeking and obtaining an understanding of the basic features of H–H and C–H activation in discrete transition metal complexes and on two transition metal surfaces.

We have learned much that is specific along the way: why an H_2 adds sideways to a 16-electron ML_5 center, the role of steric problems in CH_4 approaching a metal center, how activation is achieved on d^8 CpML fragments and how it might occur in d^{10} ML_3 and ML_2 species, how H_2 interacts initially with a Ni(111) surface and how that surface differs in electron density from a similar Ti surface, and the apparent importance of a two-metal mode of bond cleavage on the surface.

But what is most interesting about our research, we believe, is the demonstration that with proper tools it is possible to illustrate the clear and essential similarity between what happens in a discrete complex and a metal surface. Indeed, how could anything

very different happen, for the basic interactions are the same? In the process of breaking an H–H or C–H bond electrons must flow from a σ orbital to the metal, and from the metal to σ^*. The metal–H bond forms at the same time. To be sure there are differences in the pacing of these electron transfers. In transition metal complexes coordinative unsaturation is essential, and with it the initial stages of reaction are dominated by $\sigma \rightarrow M$ electron transfer. But for Ni(111) the surface is electron rich, the Fermi level is higher than for a molecule, and it is electron transfer from $M \rightarrow \sigma^*$ that dominates the early stages of the reaction.

The analytical tools we use in this paper are a density of states analysis, the projections of that density of states on various atoms and orbitals—very similar to gross atomic populations for a discrete complex. We introduce an immensely useful new indicator—the crystal orbital overlap populations or COOP curves (technically the overlap population weighted density of states). This is the solid-state analogue of a Mulliken overlap population and allows a limpid analysis of bond forming and breaking processes. These tools, along with one we did not use in this paper, the extended structure analogue of Walsh diagrams, give chemists a language for understanding solid-state structure and reactivity.

Appendix I. Extended Hückel and Geometrical Parameters

Molecular Calculations. Extended Hückel parameters for all atoms used are listed in Table VI. Idealized geometries were assumed and standard bond lengths and bond angles were used. In the ML_n (n = 2–5) fragments, all LML bond angles were 180° and 90°. The CpRhCO fragment was bent with the angle (OC)(Rh)(centroid of Cp) equal to the ideal value of 125.3°, the Rh–centroid distance being 1.85 Å. In the $Rh(C_6H_6)^-$ fragment the Rh–centroid distance was 1.82 Å. All HCH angles were assumed to be 109.47°. The following standard bond distances were used: M–CO = 1.90 Å; C–O = 1.15 Å; $Rh–CH_3$ = 1.95 Å; Rh–H = 1.60 Å; Rh–P = 2.30 Å; Rh–Cl = 2.30 Å; C-(Cp)–C(Cp) = 1.43 Å; C(benz)–C(benz) = 1.41 Å; C–H = 1.09 Å; H–H = 0.74 Å. The geometries of **17** (L = CO; R = R′ = H) and **23** were constructed from idealization of experimental structures[5a,d] with use of bond distances given above.

Bulk and Surface Calculations. All the calculations were of the tight binding extended Hückel type. The same parameters as for molecular calculations (Table VI) have been used for C and H.

The H_{ii}'s of the transition metals from Ti to Ni have been determined by charge iteration on bulk metals, assuming the charge dependence of metal H_{ii}'s given by Gray's equations.[29] The A, B, and C iteration parameters were taken from ref 30. Experimental hcp, fcc, and bcc structures were used[31] except for Mn for which a bcc structure was assumed with a lattice parameter determined by averaging those of Cr and Fe.

The extended Hückel parameters for Ti to Ni are listed in Table VII. Note that they are substantially higher in energy than the same parameters in discrete molecular complexes.

Calculations of H_2 on Ni and Ti were made assuming a two-dimensional slab of metals, four layers thick, with a 1 × 1 coverage on both sides of the slab. Calculations with H_2 on one side give very similar results. Interactions between H_2's have been dropped to simulate a low coverage. The repeating unit cell contains four Ni atoms and two H_2 molecules. A 14K point set[32] was used in

hexagonal symmetry; for lower symmetries, special point sets were generated by symmetry reduction of this hexagonal set.

Calculations of CH_4 on Ni and Ti were made with a slab of three metal layers with a ($\sqrt{3} \times \sqrt{3})R(30°)$ coverage of CH_4 on one side of the slab only. The repeating unit cell contains nine Ni atoms and one CH_4 molecule. A 5K point[32] set was used in hexagonal symmetry, from which special sets were obtained by symmetry reduction for lower symmetries.

In all calculations the H–H distance is 0.74 Å, unless otherwise specified. The C–H distances were set to 1.1 Å if they were interacting with the surface, if not they were set to 1.09 Å. HCH angles were 109.47°. The Ni–Ni and Ti–Ti distances are taken from ref 31.

Appendix II. The Film or Slab Model for Surfaces

In order to determine the best compromise between time of computation and accuracy of the model, a study of the dependence of surface electronic structure on slab thickness was undertaken. In Table VIII are listed several computed quantities for Ni(111) slabs made up of different numbers of layers. These were carried out with use of a hexagonal 30K point set.[32] Reasonable convergence is reached for a slab of four layers. Electron densities of the middle layer are not very different from those calculated for three-dimensional bulk nickel (using a 110K point set); the major difference is in the 3d population, due to the negative polarization of the surface layer described in the text.

The overlap population inside the slab is close to the one obtained for bulk Ni. That the Ni–Ni overlap population is largest on the surface may be explained by narrowing of the surface 3d band as shown in **33**: Compared to the corresponding inner slab states, the bonding surface states are less bonding and the antibonding states are less antibonding. For nickel almost all the antibonding d levels are filled. As an antibonding level is in fact more antibonding than the corresponding bonding level is bonding, the loss of antibonding character dominates on the surface, causing the increased Ni–Ni overlap population.

We also have observed that for the four-layer slab good convergence is reached for the projected DOS of the surface layer and of the middle layer. Comparison of Figures 10 and 12 shows that the projected DOS of the inner layer of a four-layer-thick slab resembles the total DOS of the three-dimensional bulk Ni.

Calculations of various geometries of H_2 on slabs of three and four layers show that, even if computed electron densities and overlap populations are slightly different, the general trend obtained for a four-layer slab is conserved for a three-layer slab.

(29) Ballhausen, C. J.; Gray, H. B. "Molecular Orbital Theory"; W. A. Benjamin, Inc.: New York, 1965, p 125.

(30) McGlynn, S. P.; Van Quickenborne, L. G.; Kinoshita, M.; Carroll, D. G. "Introduction to Applied Quantum Chemistry"; Holt, Rinehart and Winston, Inc.: New York, 1972.

(31) Donohue, J. "The Structure of the Elements"; R. E. Krieger: Malabar, 1982.

(32) Pack, J. D.; Monkhorst, H. J. *Phys. Rev. B* **1977,** *16,* 1748–1749.